The renaissance of iron-based Fischer–Tropsch synthesis: on the multifaceted catalyst deactivation behaviour†

Emiel de Smit and Bert M. Weckhuysen*

Received 7th August 2008
First published as an Advance Article on the web 14th October 2008
DOI: 10.1039/b805427d

Iron-based Fischer–Tropsch catalysts, which are applied in the conversion of CO and H_2 into longer hydrocarbon chains, are historically amongst the most intensively studied systems in heterogeneous catalysis. Despite this, fundamental understanding of the complex and dynamic chemistry of the iron–carbon–oxygen system and its implications for the rapid deactivation of the iron-based catalysts is still a developing field. Fischer–Tropsch catalysis is characterized by its multidisciplinary nature and therefore deals with a wide variety of fundamental chemical and physical problems. This *critical review* will summarize the current state of knowledge of the underlying mechanisms for the activation and eventual deactivation of iron-based Fischer–Tropsch catalysts and suggest systematic approaches for relating chemical identity to performance in next generation iron-based catalyst systems (210 references).

Introduction

In Fischer–Tropsch synthesis (FTS), syngas, a mixture of CO and H_2, is catalytically converted through a surface polymerisation reaction into a wide spectrum of hydrocarbon chains.[1,2] The most straightforward overall reaction yields straight chain alkane products:

$$n\mathrm{CO} + (2n + 1)\mathrm{H_2} \rightarrow \mathrm{C}_n\mathrm{H}_{2n+2} + n\mathrm{H_2O} \qquad (1)$$

The FTS reaction is a strongly exothermic reaction. Often the catalysts and reaction conditions are tuned in such a way to obtain a wax consisting of long hydrocarbon chain products (C_{20+}). This wax can then subsequently be cracked into the desired product hydrocarbon chain length.

FTS is a heterogeneous catalytic reaction; under typical reaction conditions the reactants and products are present in the gas (and liquid) phase and the catalyst itself is present as a solid. Iron, cobalt, nickel and ruthenium are all catalytically active in FTS. However, nickel shows undesirably high methane selectivity, while ruthenium resources are scarce and expensive, and therefore both elements are not commonly used. As a result, mainly iron and cobalt are used industrially. Except for the alkane reaction described above, depending on the process conditions and the catalysts that are used, the reaction product spectrum can also be shifted to alkenes and alcohols.

FTS makes feasible the production of practically contaminant (sulfur, nitrogen, aromatics) free transportation fuels (*e.g.* diesel) and valuable chemicals (*e.g.* short chain alkenes, oxygenates) from feedstocks alternative to oil, most notably

Inorganic Chemistry and Catalysis, Debye Institute for Nanomaterials Science, Utrecht University, Sorbonnelaan 16, 3584CA Utrecht, The Netherlands. E-mail: b.m.weckhuysen@uu.nl; Fax: +31 (0) 30 251 1027; Tel: +31 (0) 30 253 4328
† The authors gratefully acknowledge Shell Global Solutions for financial support.

Emiel de Smit

Emiel de Smit (26) earned his Masters degree from Utrecht University, The Netherlands. His Master of Science research on cobalt-based Fischer–Tropsch catalysts was carried out under the supervision of Prof. Weckhuysen. After graduating, he continued as a PhD student in the group of Prof. Weckhuysen. His primary research interest is in the use and development of the in situ *characterization tools for studying iron-based Fischer–Tropsch catalysts.*

Bert Weckhuysen

Bert Weckhuysen (40) received a Masters and PhD from Leuven University, Belgium. He has been a post-doc at Lehigh University and at Texas A&M. Weckhuysen is a full professor of Inorganic Chemistry and Catalysis at Utrecht University and scientific director of the Netherlands Institute for Research in Catalysis (NIOK). His research interests include among others renewable catalysis, environmental catalysis, catalysis for bulk chemicals and in situ *spectroscopy of catalytic solids.*

coal, biomass and natural gas. The technology related to the conversion of syngas produced from these feedstocks is referred to as gas-to-liquid (GTL), coal-to-liquid (CTL) and biomass-to-liquid (BTL), respectively.

Historically, commercial interests and research efforts in this alternative production route have often paralleled crises in the oil feedstock supply chain. A clear cut example is the production of FTS transportation fuels from coal in WWII Germany, which was cut off from oil supplies by allied forces but had large coal reserves. A few decades later, already having some experience with FTS technology, South Africa invested significant research in the FT process during its 1970s–1980s oil sanctions. During that same decade, the 1973 and 1979 energy crises initiated new worldwide initiatives for transportation fuels and chemicals from alternative feedstock, including FTS.

The overproduction of oil in the following decades and resulting lower oil prices cooled these efforts somewhat. However, during the last decade of the previous century, political conflicts in oil-rich regions, indications of depleting oil reserves, rapid growth of the Chinese and Indian economies, and the improved environmental awareness leading to the enforcement of strict greenhouse gas and sulfur emission rules revived the research efforts into FTS. The recent renaissance of the Fischer–Tropsch synthesis is not only reflected in the recent major industrial investments in the exploitation of FT production facilities,[3] but even more markedly by the almost tripled output of peer reviewed FTS research papers since 1995 (Fig. 1). Because of both the vast worldwide reserves of coal and the drive toward CO_2 neutral transportation fuels, mainly CTL and BTL can be expected to be a major part of FT applications in the future.

In addition to being very active FTS catalysts, iron-based catalysts have unique water–gas shift (WGS) capabilities, *i.e.* they catalyze the reaction between carbon monoxide and water to form hydrogen and carbon dioxide:

$$CO + H_2O \leftrightarrow H_2 + CO_2 \qquad (2)$$

Therefore these catalysts are especially suited for the production of liquid hydrocarbon products from syngas derived from sources, such as coal (CTL) and biomass (BTL), which typically have a too low H_2 to CO ratio ($H_2/CO \approx 1$) to stoichiometrically produce longer chain hydrocarbon products. Cobalt-based FTS catalysts, because of their high intrinsic activity and stability, remain the catalyst of choice for the conversion of syngas from natural gas (GTL) with its higher (stoichiometrically suitable) H_2 to CO ratio ($H_2/CO \approx 2$).

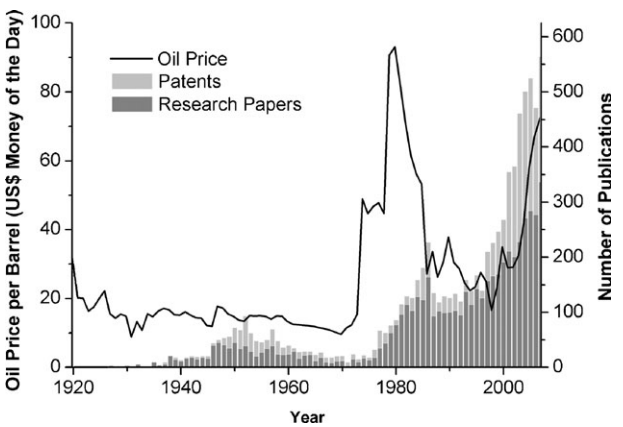

Fig. 1 Oil price (line) related to the output of peer reviewed FTS research papers and patents[4] (bars) in 1925–2007.

Iron-based FTS catalyst precursors consist of nanometre-sized Fe_2O_3 crystallites to which often promoters are added to improve the catalyst performance. A typical catalyst contains promoters like copper to enhance catalyst reducibility, potassium to improve CO dissociation, along with some silica or zinc oxide to improve the amount of iron atoms interacting with the gas phase (*i.e.* catalyst dispersion). The catalyst is treated in H_2, CO or syngas to convert it to its active form. During FTS, a complex mixture of iron phases is formed. In general, it is recognized that metallic iron, carbidic iron and iron oxides coexist after activation and during FTS. Surface carbidic iron species are believed to be the active phase since the earliest studies in the open literature. However, even after many recent detailed characterization studies, the exact identity of the active phase(s) remain(s) controversial.

In addition to the ability to catalyze the WGS reaction, iron-based FTS catalysts have the additional advantage that iron is widely available and thus catalysts are relatively cheap. Furthermore, over iron-based catalysts the FTS product spectrum can be tuned to a wider range (alcohols, alkenes, *etc.*) compared to typical cobalt-based catalysts. These advantages make the iron-based catalysts attractive candidates in the development of next generation FTS catalysts, especially for CTL and BTL technology.

The main challenge in the design of novel iron-based FTS catalysts, however, remains overcoming their notoriously high deactivation rates, which has been a subject of study in corporate research for many years. This interest may not be unexpected since, in general, rapid catalyst deactivation and the costs of catalyst replacement or regeneration that come with it are very unfavorable from a commercial point of view. However, academic research efforts and fundamental understanding into the exact pathways that are responsible for the multifaceted catalyst deactivation behaviour are remarkably scarce in the open literature.

The iron-based FTS catalyst system is one of the oldest and perhaps most studied systems known in the field of heterogeneous catalysis. However, even after more than 80 years of research, many important research questions remain unanswered. The exact structural composition of the active site in these catalysts is still not unambiguously identified and despite the research efforts into understanding mechanisms of deactivation in these catalysts, stabilization of the active catalysts still remains a vast challenge. In order to gain more insight into the deactivation behaviour of iron-based FTS catalysts, a better understanding of the precise structure and the role of the different iron (metallic, oxidic and carbidic) species formed in these catalysts during the different stages of reaction is needed. Even though the different iron bulk phases present during FTS have been identified in the earliest catalytic studies, precise structural data of these phases and especially iron carbides and their role in the activation and deactivation of iron-based FTS catalyst materials are still highly disputed in literature. Novel surface science techniques, which became available in the 70s and 80s of last century, boosted research efforts for identifying the (near) surface structure of the

catalysts and correlating them to the catalytic performance of the materials. Some combined bulk–surface studies are found in literature, however, as of today most literature on iron-based FTS catalysts is still divided into two classes: studies aiming to correlate bulk phases with catalytic performance and studies that mainly consider the correlation between surface structure and catalytic performance. Perhaps even more striking is the small number of *in situ* studies. The largest part of the literature that is available focuses on either *ex situ* or quasi *in situ* characterization of the catalyst materials, while true *in situ* studies remain very rare.

The recently renewed interest in iron-based FTS catalysts has boosted research efforts and led to many novel research approaches. This review will summarize research efforts concerning the deactivation of iron-based FTS catalysts carried out until 2007. An overview of the physical and chemical properties and the characterization methods of the iron oxide, iron and iron carbide phases found during FTS will be discussed, followed by an overview of the different viewpoints on the origin of the catalytic activity of iron-based FTS catalysts and the assumed deactivation mechanisms. Special attention will be given to the diverse role of carbon in these mechanisms. The review paper ends with a survey of the scientific challenges for the field.

Iron phases in Fischer–Tropsch synthesis: properties, synthesis and characterization

Iron oxide

General properties. Iron oxides are widespread and abundantly found in nature. The element iron is the fourth most abundant element in the earth's crust and most of it is found in the form of iron oxides. Except for being present in the earth's crust, oxides are present in almost all of the different compartments of the global system. Partially owing to their high abundance, iron oxides are widely studied and found in many applications. Research in iron oxides is spread over many different scientific disciplines, including mineralogy, geology, biology, medicine, environmental chemistry, industrial chemistry and catalysis. In the field of catalysis, except for the Fischer–Tropsch process, iron oxides (precursors) are commonly used catalysts, most notably in the synthesis of ammonia.[5]

There are sixteen iron oxides,[6] including the different iron hydroxides and iron oxide hydroxides (also referred to as oxides here for the sake of simplicity). They are summarized in Table 1. The iron oxides that are reported to be important in FTS precursors and during FTS itself, marked in italics, are α-Fe_2O_3, γ-Fe_2O_3, FeOOH, Fe_3O_4 and FeO.

All iron oxides consist of close packed arrays of anions (O^{2-} or OH^-) (usually hexagonal (hcp) or cubic (ccp) close packing) in which the iron cations, which are generally in the trivalent state, occupy the octahedral and sometimes tetrahedral spaces. The main structural differences between the different oxides arise from the way the octahedral and tetrahedral building units are organized.

The iron oxide hydroxides are easily dehydroxylated to iron oxides, owing to the similarity between the anion frameworks of these compounds, which accommodates the rearrangement of iron cations and the loss of OH in the crystal structures. Goethite, for example, transforms to hematite by losing pairs of H_2O molecules from its crystal structure, while the common anion array stays intact. Typical characteristics of the iron oxides are their low solubility in water, brilliant colors, the relative ease of replacement of iron cations by other cations (most notably Ti^{3+} and Al^{3+}), and of course their catalytic activity. Part of this catalytic activity can be ascribed to the fact that iron oxides and oxide hydroxides have a very high energy of crystallization. This causes them to grow very small crystals with high specific surface areas (usually higher than $\sim$100 $m^2\ g^{-1}$) and many exposed functional groups. Below, we will discuss the oxides that are important in FTS in more detail. Table 2 shows some important general properties of these oxides. Fig. 2 depicts selected iron oxide crystal structures.

Table 1 Iron oxides

Oxides	Hydroxides	Oxide hydroxides
Hematite α-Fe_2O_3	Ferrihydrite $Fe_5HO_8{\cdot}4H_2O$	*Goethite* α-*FeOOH*
Magnetite Fe_3O_4	Bernalite $Fe(OH)_3$	Lepidocrocite γ-FeOOH
Maghemite γ-Fe_2O_3	$Fe(OH)_2$	Akagenéite β-FeOOH
β-Fe_2O_3		Schwertmannite $Fe_{16}O_{16}(OH)_y(SO4)_z{\cdot}nH_2O$
ε-Fe_2O_3		Feroxyhyte δ-FeOOH
Wüstite FeO		δ'-FeOOH
		High pressure FeOOH

Hematite. Hematite, α-Fe_2O_3, is widespread in nature in solids and rocks. When finely divided it has a bright red colour, while it appears grey or black when very crystalline. It is isostructural with corundum and thus based on hexagonal packing (hcp) of oxygen ions. Iron oxide is (and has been for thousands of years) an important pigment and valuable ore.

Magnetite. Magnetite, Fe_3O_4, is a black ferrimagnetic material containing both Fe^{2+} and Fe^{3+} in a ratio of 1 : 2. It has an inverse spinel crystal structure with the Fe^{2+} ions occupying the octahedral sites. It is the most stable form of iron oxide under standard conditions and is commonly found in deactivated catalysts.

Maghemite. Maghemite, γ-Fe_2O_3, is a ferrimagnetic material with the same crystal structure as magnetite but without the Fe^{2+} cations. Maghemite is an important magnetic pigment and is sometimes found in deactivated FTS catalysts.

Wüstite. Wüstite, FeO, is a black iron oxide with iron cations in the Fe^{2+} state. Its structure resembles the rock salt structure and is based on a ccp anion array. In practice "pure" FeO does not exist as the crystal lattice always contains defects. Although it is not stable in air, wüstite is an important intermediate during the reduction of more oxidic iron ores to iron and it is therefore always formed during the reduction of FTS catalysts precursors.

Goethite. Goethite, α-FeOOH, like hematite is very commonly found in the earth's crust. Its structure is based on a hexagonal (hcp) packing of anions. At room temperature and standard pressure, goethite (along with hematite and magnetite) is one of

Table 2 General properties of selected iron oxides

	Hematite	Magnetite	Maghemite	Wüstite	Goethite
Crystal system	Trigonal	Cubic	Cubic or tetragonal	Cubic	Orthorhombic
Density/g cm^{-3}	5.26	5.18	4.87	5.9–5.99	4.26
Type of magnetism	Weakly ferromagnetic or antiferromagnetic	Ferrimagnetic	Ferrimagnetic	Antiferrimagnetic	Antiferrimagnetic
Standard free energy of formation ΔG_f^0/kJ mol^{-1}	−742.7	−1012.6	−711.1	−251	−488.6

the most stable oxides. In larger crystals, goethite is dark brown. Very small crystals, however, have a distinct yellow colour. Goethite is a very important industrial pigment. In FTS it is commonly found, along with hematite, in the catalyst precursor.

Synthesis. As stated above, iron oxides are very abundant in the earth's crust. This means that a large part of iron oxides can simply be extracted from the ground. Industrial synthesis, however, is very common as well because of the high purity and morphology requirements for specialty iron oxides (*e.g.* paint pigments, magnetic pigments). The starting materials for industrial processes, as opposed to laboratory use, are usually Fe^{2+} salts rather than Fe^{3+} salts because the former are cheaper. Three major synthesis routes are used in industry:

1. Solid state transformation, including thermal decomposition.
2. Organic reduction processes, in which metallic iron is oxidized to iron oxide by an organic oxidizer (*e.g.* nitrobenzene).

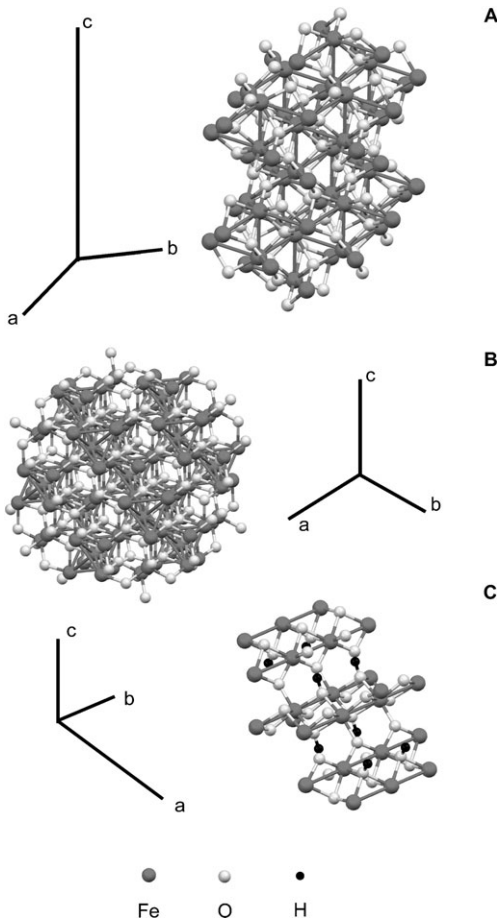

Fig. 2 Representation of structures of: (A) hematite, (B) magnetite and (C) goethite. The unit cell axes are indicated next to the structures.

3. Precipitation of soluble iron salts with alkali salts, followed by oxidation.

Other industrial routes include hydrothermal precipitation, flame hydrolysis, thermal decomposition of $Fe(CO)_5$ and high temperature reaction of Fe^{3+} chloride with iron.

There are many ways of synthesizing iron oxides in the laboratory.[7] However, the most common method for the synthesis of catalyst precursors is basic precipitation from iron (3+) salt solutions. Many FTS catalyst precursors, for example, are synthesized by adding an iron nitrate solution to a sodium carbonate solution.[8] Alternatively, they are also produced by electrical fusing. Several examples of the preparation of iron oxide FTS catalyst precursors are described in detail in literature.[8–10]

Characterization. Iron oxides are well studied and the different iron oxides are readily distinguished by most characterization techniques. The most commonly applied techniques to study iron oxides are: infrared spectroscopy (IR), Mössbauer spectroscopy (MES), ultraviolet-visible (UV-Vis) spectroscopy and X-ray diffraction (XRD). Raman spectroscopy (RS), X-ray photoelectron spectroscopy (XPS), Auger electron spectroscopy (AES), secondary ion imaging mass spectrometry (SIMS), electron spin resonance (ESR) and X-ray absorption spectroscopy (XAS) and temperature programmed reduction (TPR) are somewhat less widely applied, but nevertheless can provide useful complementary information about the different oxides. Table 3 shows an overview of the different characterization techniques and their potential for distinguishing the iron oxidation state, coordination and phase identification.

The characteristic spectral features of the commonly observed iron oxide phases in FTS are summarized in Table 4 for the most commonly applied characterization techniques. Although direct determination of the oxidation state of iron is not possible with this technique, XRD remains the characterization tool of choice in most studies. The technique offers quick identification and an indication of size of the

Table 3 Iron oxide characterization tools and their potential

Technique	Oxidation state	Coordination	Identification
IR	+	+	+
RS	+	+	+
XRD	–	+	+
MES	+	+	+
UV-Vis	+	+/–	+/–
XPS/AES	+	–	+/–
SIMS	–	+/–	–
ESR	+	+	+
XAS	+	+	+
TPR	+	–	+/–

crystalline phases present. MES is especially useful for identifying less crystalline samples and offers direct information about the magnetic properties and oxidation state of the studied material. XAS can also provide valuable information on more amorphous iron oxide materials where information about the oxidation state of iron can be determined from the XANES region, while the EXAFS region offers information about coordination numbers and bond lengths involved. Band assignment in IR and RS is not always straightforward since it is frequently reported that crystallite size and morphology can

Table 4 Signatures of selected iron oxides for commonly applied characterization techniques

Phase	XRD	(*hkl*)	IR[11,12,23–29]	Origin	Raman[30,31] [b]	XPS[32,33]	Origin	XANES[34–36]	Origin	Mössbauer[37,38]	Parameter
α-Fe_2O_3 (13-534)[a]	d = 2.69 Å, I = 100	(104)	3720, 3700, 3635, 3490, 3435, 3380 cm^{-1}	FeO–H	613, 500, 412, 299, 247, 225 cm^{-1}	711.0 eV	$Fe(2p_{3/2})$	7123.1 eV	1s → 4p	0.37 mm s^{-1}	Isomer shift
	d = 2.51 Å, I = 50	(110)	650, 575, 525, 485, 440, 400, 385, 360, 300 cm^{-1}	Fe–O		55.7 eV	$Fe(3p_{3/2})$	7113.47 eV	1s → 3d	−0.197 mm s^{-1}	Quadrupole splitting
	d = 2.201 Å, I = 30	(113)				93.6 eV	Fe(3s)			51.8 T	Hyperfine field
	d = 1.838 Å, I = 40	(024)				529.8 eV	O(1s)				
	d = 1.690 Å, I = 60	(116)									
	d = 1.484 Å, I = 35	(214)									
	d = 1.452 Å, I = 35	(300)									
γ-Fe_2O_3 (25-1402)[a]	d = 2.95 Å, I = 30	(220)	3740, 3725, 3675, 3640 cm^{-1}	FeO–H	740, 650, 505, 380, 350, 263, 252, 193 cm^{-1}	711.0 eV	$Fe(2p_{3/2})$	—	—	0.32 mm s^{-1}	Isomer shift
	d = 2.514 Å, I = 100	(311)	700, 660–640, 620, 580, 560, 460, 430, 390, 305 cm^{-1}	Fe–O		55.7 eV	$Fe(3p_{3/2})$	—	—	0.02 mm s^{-1}	Quadrupole splitting
	d = 1.604 Å, I = 20	(511)				93.6 eV	Fe(3s)			45–52 T	Hyperfine field
	d = 1.474 Å, I = 40	(440)				530.0 eV	O(1s)				
α-FeOOH (29-713)[a]	d = 4.183 Å, I = 100	(110)	3660, 3484 cm^{-1}	FeO–H	560, 470, 385, 300, 250 cm^{-1}	711.9 eV	$Fe(2p_{3/2})$	7123.5 eV	1s → 4p	0.37 mm s^{-1}	Isomer shift
	d = 2.693 Å, I = 35	(130)	892, 795 cm^{-1}	Fe–OH		56.6 eV	$Fe(3p_{3/2})$	7113.58 eV	1s → 3d	−0.26 mm s^{-1}	Quadrupole splitting
	d = 2.450 Å, I = 50	(111)	630, 495, 449 cm^{-1}	Fe–O		94.2 eV	Fe(3s)			38.2 T	Hyperfine field
	d = 2.190 Å, I = 18	(140)	397, 263 cm^{-1}	Fe–OH		530.3 eV	O(1s)				
	d = 1.719 Å, I = 20	(221)									
Fe_3O_4 (19-629)[a]	d = 2.967 Å, I = 30	(220)	580, 400 cm^{-1}	Fe–O	676, 550 cm^{-1}	708.3 eV	$Fe(2p_{3/2})$	7123.0 eV	1s → 4p	0.26 mm s^{-1}	Isomer shift
	d = 2.532 Å, I = 100	(311)				53.9 eV	$Fe(3p_{3/2})$	7113.0 eV	1s → 3d	−0.02 mm s^{-1}	Quadrupole splitting
	d = 2.099 Å, I = 20	(400)				530.2 eV	O(1s)			49.0 T	Hyperfine field
	d = 1.612 Å, I = 30	(511)									
	d = 1.484 Å, I = 40	(440)									
FeO (6-615)[a]	d = 2.490 Å, I = 80	(111)	490, 400–250 cm^{-1}	Fe–O	210, 390, 480, 652 cm^{-1}	709.5 eV	$Fe(2p_{3/2})$	7119.3 eV	1s → 4p	0.95 mm s^{-1}	Isomer shift
	d = 2.153 Å, I = 100	(200)				54.9 eV	$Fe(3p_{3/2})$	7112.5 eV	1s → 3d	0.44 mm s^{-1}	Quadrupole splitting
	d = 1.523 Å, I = 60	(220)				92.5 eV	Fe(3s)				
	d = 1.299 Å, I = 25	(311)				530.0 eV	O(1s)				

[a] Joint committee on powder diffraction standard card #. [b] All indicated vibrations originate from Fe–O bonds.

influence the occurrence and position of vibrational bands.[11,12] It can be seen from the table that XPS analysis of iron oxides is hampered by the fact that the oxygen 1s transition is very similar in all oxides, except for α-FeOOH.

The role of iron oxides in Fischer–Tropsch synthesis. Small iron oxide crystallites, either present as hematite/goethite or magnetite, constitute the FTS catalyst precursor. High performance FTS catalysts are characterized by their high specific surface area (~150 m^2 g^{-1} for bulk, ~300 m^2 g^{-1} for silica-bound catalysts) stemming from the complex structure of agglomerates of ~10–50 nm primary particles of iron oxide. Except for the fact that iron oxide is the FTS catalyst precursor, iron oxide in the form of magnetite plays an important role. It is well known that magnetite catalyzes the water–gas shift (WGS) reaction (eqn (2)).[13] It is therefore thought to be the phase responsible for the WGS activity of iron-based FTS catalysts.[13–18] Generally speaking, it is accepted in the literature that the WGS reaction and the FTS reaction take place on different types of active site on the catalyst. Since magnetite is known to co-exist with other iron phases during FTS, it plays an important role in determining the overall activity and selectivity of the catalyst. Magnetite has in some cases also been reported as an active phase in FTS.[19–22]

Metallic iron

General. Elemental iron is almost never found as such in nature. All metallic iron has to be produced by the reduction of iron ores. Owing to the high abundance of iron ores, the relative low cost of the reduction process and its high strength, iron is the most frequently used metal in metal (alloy) applications and comprises a staggering 95% of all the metal tonnage produced worldwide. In modern society it is indispensable, especially in applications like automobiles, the hulls of large ships, and structural components for buildings. The most common form of pure metallic iron found at low to moderate temperatures (<723 °C), α-Fe or ferrite (soft iron), has the body centered cubic (bcc) crystal structure. At higher temperatures, face centered cubic (fcc) iron, γ-Fe or austenite (hard iron) is formed. Fig. 3 shows the crystal structures of both forms of iron. In FT catalysis, the commonly reported crystal structure of iron is α-Fe. Chemically, elemental iron, along with all transition metals that come earlier in the series, is known for its ability to dissociate CO at room temperature and is able to dissolve carbon in its crystal interstices, forming carbides. α-Fe can dissolve only 0.02 wt% C before being transformed into a mixture of α-Fe and θ-Fe_3C (cementite).

Synthesis. The production of metallic iron is the most important application of carbon metallurgy. Industrially, metallic iron is almost exclusively made using the blast furnace process. In the furnace a mixture of iron ores (Fe_2O_3 and Fe_3O_4), coke and limestone ($CaCO_3$) is heated in hot air. The coke combusts in the hot air to CO and raises the temperature in the oven to about 2000 °C. The CO then reacts with the iron oxides, which are added from the top of the furnace. The iron oxides are reduced to Fe through Fe_3O_4 and FeO. The limestone is added to form CaO and combine with any silicate

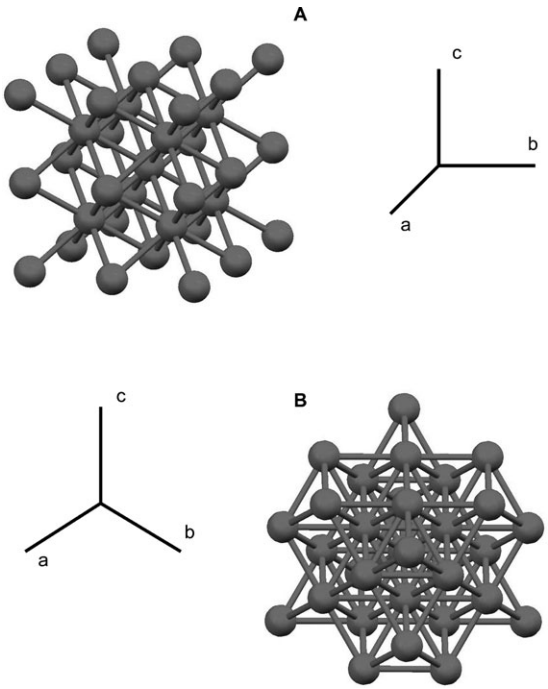

Fig. 3 Representation of the crystal structures of: (A) bcc α-Fe and (B) fcc γ-Fe. The unit cell axes are indicated next to the structures.

contaminants present in the iron ore. In catalysis, reduction of iron oxides can be carried out under substantially milder conditions and reductions are typically done under a hydrogen atmosphere at temperatures around 250–350 °C. The iron oxide precursor Fe_2O_3 undergoes transformations to Fe_3O_4 and FeO before being fully reduced to α-Fe. H_2O can readily oxidize metallic iron at higher temperatures. Because H_2O is produced during reduction, the H_2 : H_2O partial pressure ratio plays an important role in the reduction process. Thermodynamics dictate that in a gaseous environment with a H_2/H_2O ratio of 1, reduction to metallic iron is impossible below 1000 °C.[39] For that reason, sometimes it can be advantageous to use gaseous CO as a reductor instead of H_2.

Characterization. Metallic iron is readily detected by many characterization techniques. The most commonly applied techniques are: XRD, MES, XPS, AES, ESR and XAS. Table 5 summarizes characteristic features of iron phases in commonly applied characterization techniques.

For an extensive review on the characterization of iron surfaces and their interaction with reactive gases, the reader is referred elsewhere.[39]

The role of iron in Fischer–Tropsch synthesis. In FTS catalysis, α-Fe is produced by reducing Fe_2O_3/Fe_3O_4/FeOOH catalyst precursors under a H_2 atmosphere at low temperatures (250–300 °C). The formed phase is reported to be very active in FTS; however, this is not a generally accepted fact in the literature. The exact role of metallic iron in FTS is multifaceted and complicated, as will be discussed in more detail later on in this review.

Table 5 Signatures of α-Fe and γ-Fe for commonly applied characterization techniques

Phase	XRD	(*hkl*)	XPS[21,22,40]	Origin	XANES[b 41]	Mössbauer[c 21,42,43]
α-Fe (6-696)[a]	d = 2.0268 Å, I = 100	(110)	706.6 eV	Fe($2p_{3/2}$)	7112.0 eV	~0.006–0.15 mm s^{-1}
	d = 1.4332 Å, I = 20	(200)	707.4 eV	Fe($2p_{3/2}$)		~31–33 T
	d = 1.1702 Å, I = 30	(211)	720.0 eV	Fe($2p_{1/2}$)		
			90.8 eV	Fe(3s)		
			52.4 eV	Fe(3p)		
γ-Fe (33-397)[a]	d = 2.08 Å, I = 100	(111)			7112.0 eV	
	d = 1.800 Å, I = 80	(200)				
	d = 1.270 Å, I = 50	(220)				

[a] Joint committee on powder diffraction standard card #. [b] K-edge energy position. [c] Isomer shift and hyperfine field.

Iron carbides

General. Carbides can be classified as covalent (*e.g.* SiC), ionic (*e.g.* CaC_2) or interstitial carbides (*e.g.* WC). The size and electronegativity of transition metals place them in either the ionic or interstitial class of carbides. Many early transition metals are able to interstitially dissolve small atoms, such as carbon, oxygen or nitrogen, into their crystal lattices. Transition metals that have interstitially dissolved carbon in their crystal lattice are referred to as transition metal carbides (TMC). These transition metal carbides often have unique chemical and physical properties.[44,45] Many TMC compounds are reported to have high melting points (>3000 °C), hardness (>2000 kg mm^{-2}) and tensile strength (>300 GPa) in the range of ceramic materials. These properties are often taken advantage of in applications like cutting tools and structural building components. However, even though the physical properties of these materials are much like other "classical" ceramic compounds, electronically and magnetically these materials still resemble metals.

TMC compounds of early transition metals (group IV, V, VI with the exception of Cr) often adopt simple crystal structures much like pure metals. The metal atoms are ordered in face centered cubic (fcc), hexagonal close packed (hcp) or simple hexagonal structures, while the carbon atoms occupy the interstitial sites. Usually, only the largest sites available are occupied: octahedral for fcc/orthorhombic and trigonal prismatic for hcp and hexagonal structures. The structure that the carbide adopts is determined by two factors: geometric and electronic factors.[46] The geometric factor can be summarized by an empirical rule found by Hägg. This rule states that if the ratio of nonmetal to metal hard-ball radii is less than 0.59, simple structures as mentioned above are formed. The electronic factor can be described by the Engel–Brewer theory of metals.[47,48] Bonding in interstitial compounds takes place through interaction between the s–p orbitals of the nonmetal and the s–p–d band of the metal atoms. The Engel–Brewer theory states that the structure that is adopted by a metal or alloy is dependent on the s–p electron count. With increasing values of this count the crystal structure is predicted to transform from bcc to hcp to fcc. Such a trend is observed upon moving from left to right in the periodic table for early second and third row transition metal elements. The later transition metals such as Fe, Co, Ni, Mn and Cr have somewhat lower hard-ball radii and do not form typical interstitial carbides. In these carbides, the metal lattices are distorted and, unlike their early TMC counterparts, carbon atoms interact with each other directly. They roughly resemble a distorted metal lattice with chains of carbon atoms running through them. These TMC species often do not show the same properties (high melting point, tensile strength, *etc.*) as the early TMC compounds and are best looked upon as a mixture between ionic (*e.g.* CaC_2) and interstitial carbides.

When considering the catalytic properties of TMC compounds, an obvious property to take a closer look at is the influence of the addition of carbon on the d-band occupation and the Fermi level of the metals. XPS[49,50] and X-ray emission spectroscopy (XES)[51] results for early TMC compounds have shown evidence that electrons are donated from the metal atom to the carbon atom. The binding energy of the electrons is shifted towards higher energies in the carbidic state, indicating charge transfer from the carbon to the metal atom. In Fe-based catalysts, this shift has hardly ever been observed, most probably due to the large amounts of free carbon covering the iron carbide material.

In a landmark publication by Levy and Boudart,[52] it was first noted that the carbides of tungsten chemically (catalytically) behaved very much like platinum metal by catalyzing the reaction of H_2 and O_2 at room temperature, unlike the parent tungsten metal. Ever since this discovery, carbides have been of great interest for studying catalytic reactions and often the activity, selectivity and resistance to poisoning of TMC compounds have been reported to surpass the properties of the best known group VIII catalysts for hydrogenation reactions.[46,53,54] It has been noted that TMC compounds, because of their refractory nature are very potent heterogeneous catalysts because of enhanced attrition (*i.e.* breaking up of catalyst particles into smaller particles) and sintering (*i.e.* loss of catalytically active surface area) resistance.[55] In this respect, it has to be noted that the research until today has primarily focused on the catalytic properties of early transition metal carbides. As TMC compounds like to form with low surface areas and are easily contaminated by free carbon or oxygen on the surface, the main challenges in the application of TMC catalysts deal with these problems.[56,57] A wealth of information is available on the electronic and physical properties of early TMC compounds, but very little fundamental research has been done on the electronic structure and physical properties of iron carbide species with respect to catalysis. This is even more surprising as many have underlined the importance of iron carbide phases for FTS; in the words of Leclercq:[56] "It is not yet clear precisely which role, (iron (ed.)) carbides play in the (Fischer–Tropsch (ed.)) synthesis, but at least their formation has a profound effect on the iron environment

and highlights an important modification of catalytic activity of parent metal by alloying with carbon".

An interesting view on the Fischer–Tropsch activity of TMC compounds is given in the work done on molybdenum carbide hydrogenation catalysts.[57–60] Shultz *et al.*[58] first investigated the catalytic properties of molybdenum metal carbides and concluded that they showed moderate FTS activity. Leclercq *et al.*[57] and Saito and Anderson[59] investigated, amongst other compounds, unsupported molybdenum carbide, oxide and nitride compounds. These investigators found that the specific activities of these compounds (based on the number of active sites) were comparable to the best metallic catalysts. However, as mentioned before, most of these materials showed low surface areas resulting in limited contact between the catalyst surface and reacting gas atmosphere. As a consequence only moderate catalyst time yields were observed. In spite of the moderate activity of these materials, though, molybdenum-based catalysts have good sulfur tolerance and are good water–gas shift catalysts. Therefore, they can be applied for the conversion of hydrogen lean synthesis gas and without the need for expensive sulfur removal processes often required for other catalysts. The sulfur poisoning resistance of iron carbides has been illustrated by Madon and Shaw.[61] They found that the carburized iron FTS catalysts required twice the amount of sulfur compared to reduced iron catalysts. Addition of small amounts of H_2S to the gas flow even was observed to improve the C_{5+} selectivity (percentage of CO converted to hydrocarbon chains of five carbon atoms and longer) of the catalysts. Something that was confirmed much later in a paper by Wu *et al.*[62] We will elaborate further on the role of sulfur in iron catalysts later in the review. One final remarkable property that most TMC compounds seem to have in common is that even at high temperatures and high H_2 : CO ratios longer hydrocarbon chains are produced, in contrast to, for example, nickel- and ruthenium-based catalysts. Substantial research efforts by the US Bureau of Mines from 1948–1963[63] on the preparation and testing of iron carbide, nitride and mixed phases have illustrated that all the bulk carbides (and nitrides and carbonitrides) of iron are active catalysts in FTS.

Iron carbides can adopt various structures which can be classified according to the sites occupied by the carbon atoms: structures with carbon atoms in trigonal prismatic (TP) interstices and structures with carbon atoms in octahedral interstices. (Pseudo-)cementite (θ-Fe_3C),[64] Hägg carbide (χ-Fe_5C_2)[65,66] and Fe_7C_3[67,68] have been well known carbides in FTS of the former class since the first characterization studies. These carbides usually have stable and clearly established structures. This is not always the case for the metastable carbides, such as ε-Fe_2C[69] and ε′-$Fe_{2.2}C$,[70,71] which have carbon atoms in the octahedral interstices. For these carbides, a complete characterization is difficult mainly because of the small particle sizes which are involved. Because the early work on the identification of iron carbides largely depended on XRD characterization, these metastable phases were not found until more recent studies. In a critical paper, Le Caër *et al.*[72] characterized by MES metastable iron carbides in FTS catalysts. Because MES is able to detect less crystalline phases as compared to the XRD technique, many other iron carbide phases have been identified since the first application of this technique as a research tool on iron-based FT catalysts. ε-Fe_2C, ε′-$Fe_{2.2}C$, Fe_7C_3, χ-Fe_5C_2, θ-Fe_3C and Fe_xC are the commonly reported carbide phases.

Table 6 shows a summary of some characteristics of the iron carbide phases found in FTS catalysts. Fig. 4 shows the crystal structures of χ-Fe_5C_2 and θ-Fe_3C. Fe_xC (or Fe_xC_y) is usually used to refer to a poorly defined iron carbide structure. Niemantsverdriet *et al.*[70] concluded from MES that the carbide was only observed in coexistence with α-Fe or just after this phase disappeared. Therefore, they concluded that the carbide was probably a poorly defined intermediate between α-Fe and a known carbide structure.

Synthesis. Most iron carbide catalysts are made *in situ* during activation treatment or under FT reaction conditions. Some preparation methods for making different iron carbides are available in the literature.[63,73–76] Hexagonal ε-Fe_2C is transformed into χ-Fe_5C_2 Hägg carbide above 250 °C, which is eventually decomposed into θ-Fe_3C cementite above 450 °C. It must be noted here that the rates of (trans)formation vary strongly with the crystallite size and impurities present. Therefore, the kinds of carbides that are formed during FTS reaction/pretreatment are expected to vary with catalyst preparation procedures. Hexagonal ε-Fe_2C can be prepared by carburizing finely divided iron or iron oxide powder at low temperatures (typically 170 °C, lower if iron is used) in a flow of CO.[76]

χ-Fe_5C_2 can be made readily by carburizing iron powder at temperatures around 250 °C.[76] Alternative synthesis methods are described by Shultz *et al.*[63] In the first method, a reduced fused iron catalyst was exposed to CO with an gas hourly space velocity of 100 h^{-1}, while heating the catalyst from 150 °C to 350 °C at such a rate to maintain a CO_2 content of 20% in the reactor exit gas. The synthesis took approximately 20 h to complete. The second method involved the carburization of the freshly reduced catalyst in a gas mixture of H_2 and CO (ratio 1 : 4). The temperature was raised stepwise: 12 h at 200 °C, 12 h at 250 °C and 12 h at 275 °C, leading to good

Table 6 Iron carbide phase characteristics

		Formula	Atomic ratio (C : Fe)	Crystal lattice	Interstitial occupation of carbon atoms	Wt% carbon
Hexagonal carbide	ε	Fe_2C	0.50	hcp to monoclinic	Octahedral	9.7
	ε′	$Fe_{2.2}C$	0.45	hcp	Octahedral	8.9
Eckstrom and Adcock carbide		Fe_7C_3	0.43	Orthorhombic	Trigonal prismatic	8.4
Hägg carbide	χ	Fe_5C_2	0.4	Monoclinic	Trigonal prismatic	7.9
Cementite	θ	Fe_3C	0.33	Orthorhombic	Trigonal prismatic	6.7
		Fe_xC				

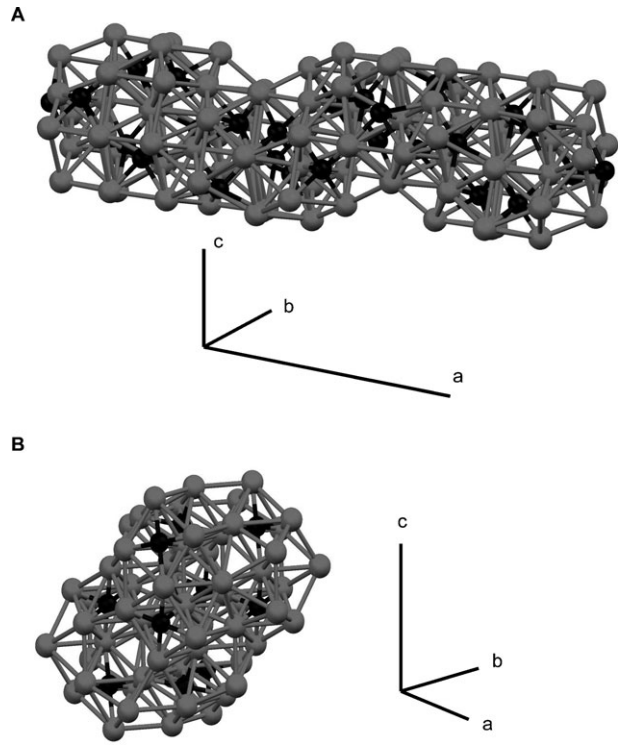

Fig. 4 Representations of the crystal structures of: (A) χ-Fe_5C_2 and (B) θ-Fe_3C. The unit cell axes are indicated next to the drawings.

yields of χ-Fe_5C_2. θ-Fe_3C can be prepared by carburizing reduced iron in syngas at temperatures above 300 °C or in methane at 500 °C. However, the carbides prepared in this way are contaminated by "free" carbon.[63,76] Another approach of preparing Fe_3C is to react iron powder with the Hägg χ-Fe_5C_2 carbide above 260 °C.[73]

Characterization. Bulk iron carbides can readily be distinguished by XRD. Most of the aforementioned iron carbides have distinct XRD diffractograms. Unsurprisingly, in catalysis, XRD analysis of carbides is one of the most applied techniques for characterization purposes.[20,42,70,77–100] However, most analyses are complicated by the fact that the carbides formed are usually very small and therefore the Bragg reflections are broadened and lower in intensity. The metastable carbides are more difficult to characterize by XRD because they have the most distorted crystal structures.

Other techniques that have been applied to study carbides are MES,[34,42,70,77,81–84,88,92,93,96,99,101–111] XPS/AES,[20,40,83,84,100,106,112–114] TEM and, more recently, scanning transmission electron microscopy-electron energy loss spectroscopy (STEM-EELS)[100,115] and XAS.[34,116–118] Table 7 shows an overview of the signatures of iron carbide phases in different characterization techniques.

Two principal challenges in studying carbides can be formulated. First, small iron carbide clusters are usually pyrogenic and they are therefore readily transformed into iron oxides when exposed to air. Some studies even observed transitions in the iron carbide structures upon cooling. A second challenge is distinguishing between bulk and surface carbides. Some papers have dealt with the air sensitivity of carbides specifically and expressed the need for improved methods to study iron carbides.[119] Part of the controversy found in the literature on active phases in iron-based FTS catalysts can be traced back to the fact that the catalyst changes between (pre)treatment and analysis. Iron carbides

Table 7 Signatures of selected iron carbides for the most commonly applied characterization techniques

Phase	XRD[67,70,71,123]	(*hkl*)	XPS[20,22,40,112]	Origin	Mössbauer[70,72,101,124]	Parameter
ε′-$Fe_{2.2}C$ (36-1249)[a]	d = 2.385 Å, I = 25	(100)			0.50 mm s^{-1}	Isomer shift
	d = 2.175 Å, I = 25	(002)			173 T	Hyperfine field
	d = 2.091 Å, I = 100	(101)			0.25 mm s^{-1}	Isomer shift
					189 T	Hyperfine field
Fe_7C_3 (17-0333)[a]	d = 2.250 Å, I = 35	(210)				
	d = 2.115 Å, I = 45	(102)				
	d = 2.012 Å, I = 100	(211)				
	d = 1.801 Å, I = 30	(301) (202)				
	d = 1.716 Å, I = 15	(220)				
χ-Fe_5C_2 (36-1248)[a]	d = 2.285 Å, I = 25	(020)	720.3 eV	Fe $2p_{1/2}$	0.46 mm s^{-1}	Isomer shift
	d = 2.207 Å, I = 50	(11-2) (202)	707.3 eV	Fe $2p_{3/2}$	189 T	Hyperfine field
	d = 2.113 Å, I = 25	(112)	91.4 eV	Fe 3s	0.51 mm s^{-1}	Isomer shift
	d = 2.081 Å, I = 80	(021)	53.0 eV	Fe 3p	218 T	Hyperfine field
	d = 2.047 Å, I = 100	(510)	283.2 eV	C 1s	0.23 mm s^{-1}	Isomer shift
	d = 2.011 Å, I = 30	(40-2) (31-2)			216 T	Hyperfine field
	d = 1.986 Å, I = 20	(22-1) (51-1)				
θ-Fe_3C (35-0772)[a]	d = 2.259 Å, I = 20	(002)			0.45 mm s^{-1}	Isomer shift
	d = 2.215 Å, I = 20	(201)			212 T	Hyperfine field
	d = 2.102 Å, I = 60	(211)			0.44 mm s^{-1}	Isomer shift
	d = 2.064 Å, I = 60	(102)			208 T	Hyperfine field
	d = 2.027 Å, I = 55	(220)				
	d = 2.011 Å, I = 100	(031)				
	d = 1.974 Å, I = 55	(112)				
Fe_xC_y			710.2 eV, 706.9 eV	Fe $2p_{3/2}$		
			284.6 eV, 284.2 eV	C 1s		

[a] Joint committee on powder diffraction standard card #.

are readily oxidized in air at room temperature,[119,120] leading to the formation of mainly Fe_3O_4.

Less has been reported on the temperature sensitivity of carbides, even though for MES usually samples are cooled down from typical FTS temperatures before analysis. Interestingly, Jin *et al.* observed by STEM the deposition of carbonaceous layers on the iron carbide particles when they cooled their samples to room temperature.[100] It was suspected that carbon in the iron carbides, present at near saturation conditions under reaction temperatures, precipitated on the catalyst surface when the samples were cooled. Both the air and temperature sensitivity of carbides appeal for the use of true *in situ* studies when studying iron catalysts.

The second issue, how to distinguish between bulk and surface carbide species, is harder to solve. It has been established that the working iron-based FTS catalysts comprise a surface iron carbide phase with an underlying bulk iron carbide structure.[42,75,101,121] However, the chemical identity of this surface carbide layer and the role of the underlying bulk carbide structure are still uncertain. One could think of applying surface sensitive spectroscopic techniques to study these systems in more detail. Soft X-ray methods, "*in situ*" XPS[122] as well as surface enhanced MES, could be promising techniques in this respect.

The role of iron carbides in FTS. The exact mechanism for the production of hydrocarbons over iron carbide phases is largely unknown. Even though it is observed that carburized iron is an active catalyst, it is still disputed in the literature whether or not bulk carbides phases themselves play an active role in the synthesis. The question on why iron does form bulk carbides under FTS conditions and the other active materials do not has been addressed by Niemantsverdriet and Van der Kraan.[125] As they pointed out, the apparent activation energy of carbon diffusion in Fe (43.9–69.0 kJ mol^{-1}) is substantially lower than for Ni and Co (138–146 and 145 kJ mol^{-1}, respectively).[126] The activation energies for the FTS reaction are very similar for the three metals.[127] For Fe, Co, Ni, they are 89.1 ± 3.8, 105 ± 5.0 and 113 ± 18 kJ mol^{-1}, respectively. In the case of Fe, the activation energy for carbon diffusion is lower than for the FTS reaction. Since for this case the exponential factors are equal within a factor of 40, the activation energies can be directly related to the reaction rates. This means that the reaction rate for the carbon diffusion reaction is higher than the rate of the FTS reaction for iron. Because of this, during the early stages of reaction, iron undergoes an induction period, in which surface carbon species are scarce and FTS activity is low. For cobalt and nickel, carbon diffusion rates are a factor 10^5 lower than for iron. Therefore the carbon diffusion rate is negligible and all carbon is converted into FTS products. Hence, although Ni reacts with CO at 250–270 °C to form Ni_3C,[128] and for cobalt Co_2C or Co_3C are stable between 500–800 °C,[129] no such phases have been reported during FTS. Many authors claim that iron carbides are absolutely necessary for a FTS catalyst to be active. However, this is still disputed by others, who believe that metallic iron is the active phase in FTS. This debate merits further discussion.

Proposed active phases and reaction mechanisms for Fischer–Tropsch synthesis on Fe-based catalysts

The general reaction equations for the synthesis of alkanes (paraffins), alkenes (olefins) and oxygenates over iron-based catalysts can be written as:

$$n\mathrm{CO} + (2n + 1)\mathrm{H_2} \rightarrow \mathrm{C}_n\mathrm{H}_{2n+2} + n\mathrm{H_2O} \quad (3)$$

$$n\mathrm{CO} + 2n\mathrm{H_2} \rightarrow \mathrm{C}_n\mathrm{H}_{2n} + n\mathrm{H_2O} \quad (4)$$

$$n\mathrm{CO} + 2n\mathrm{H_2} \rightarrow \mathrm{C}_n\mathrm{H}_{2n+2}\mathrm{O} + (n-1)\mathrm{H_2O} \quad (5)$$

Iron-based FTS catalysts generally also catalyze the water–gas shift (WGS) reaction:

$$\mathrm{CO} + \mathrm{H_2O} \leftrightarrow \mathrm{CO_2} + \mathrm{H_2} \quad (6)$$

therefore, the main oxygenated products evolving after reaction are H_2O and CO_2.

Active phases

As was already mentioned above, most iron-based FTS catalyst precursors consist of iron oxides. During catalyst activation, dependent on the gas composition and treatment temperatures used, the following chemical transitions can take place in the catalyst:

$$\mathrm{Fe}_x\mathrm{O}_y + y\mathrm{H_2} \leftrightarrow x\mathrm{Fe} + y\mathrm{H_2O} \quad (7)$$

$$\mathrm{Fe}_x\mathrm{O}_y + y\mathrm{CO} \leftrightarrow x\mathrm{Fe} + y\mathrm{CO_2} \quad (8)$$

Metallic iron species can subsequently adsorb CO on one of its active surface sites (represented by *) and subsequently dissociate it. The adsorbed carbon species can then further react with the iron species to form iron bulk carbides:

$$* + \mathrm{CO}^* \xrightarrow{k_\mathrm{d}} \mathrm{C}^* + \mathrm{O}^* \quad (9)$$

$$y\mathrm{C}^* + x\mathrm{Fe} \xrightarrow{k_\mathrm{b}} \mathrm{Fe}_x\mathrm{C}_y \quad (10)$$

where k_d and k_b are the rate constants for the dissociation and bulk carburization reactions, respectively.

As was noted before, the bulk carburization reaction (eqn (10)) has a low apparent activation energy (43.9–69.0 kJ mol^{-1}) and takes place readily on iron at typical FT reaction temperatures. Dissociated CO can, however, also be converted in two other reactions. First, if hydrogen is present, hydrogen molecules can be dissociated on the catalyst surface and surface carbide species can be hydrogenated:

$$\mathrm{C}^* + x\mathrm{H}^* \xrightarrow{k_\mathrm{h}} \mathrm{CH}_x^* + x^* \quad (11)$$

where k_h is the rate constant for the hydrogenation reaction. The CH_x species can then further react with each other on the surface, forming longer hydrocarbon chain products. Secondly, when more and more carbon species are available on the surface and hydrogen adatoms are sparse, a side reaction can take place which involves the direct coupling of carbon atoms:

$$\mathrm{C}^* + \mathrm{C}^* \xrightarrow{k_\mathrm{c}} \mathrm{C}_\mathrm{i}^* \quad (12)$$

where k_c is the rate constant for this reaction and C_i stands for inactive surface carbon species. The build-up of these species on

the catalyst surface can lead to the blocking of active surface sites, lowering the overall catalyst activity.

Under FTS working conditions, the iron-based catalyst is known to form many co-existing phases, including α-Fe, Fe_3O_4 and iron carbides. The exact role of these phases in FTS, however, remains controversial. Claims of catalytic activity of Fe_2O_3,[130] Fe_3O_4,[19–22,111] α-Fe,[70,131,132] and iron carbides[42,83,92,101,131] in FTS are all found in the literature. Even the role of the specific carbide species has been the subject of debate.[42,133] There are three main models that are used to explain the catalytically active phases of iron-based FTS catalysts and their time dependent behaviour. These models, first distinguished by Niemantsverdriet and Van der Kraan,[125] all use the four elementary reaction steps mentioned above (the full proposed mechanisms of the Fischer–Tropsch reaction will be considered later). Scheme 1 illustrates the different proposed models for the active iron-based FTS catalysts.

One model, better known as the "competition model",[70] appoints surface iron species to be the active sites in FTS. In this model, bulk carburization (eqn (10)) and FTS have the same common surface carbide precursor and there is competition between the carburization of the iron phase, the hydrogenation of surface carbon and the formation of inactive surface carbon by reaction between adsorbed carbon atoms. Carbon monoxide dissociation is assumed to be slower than the subsequent reactions. A second model,[42,92,101] dubbed the "carbide model" considers surface carbides with an underlying iron carbide bulk structure to be the active phase. Metallic iron is assumed to be inactive for FTS. In this model, the bulk carbide phase plays an important role in FTS in controlling the number of active surface sites, rather than being a spectator phase. In the third model, the "slow activation" model[70] CO dissociation is assumed to be very fast. Hence, sufficient carbon is assumed to be present for both carburization and hydrocarbon synthesis. Surface complexes consisting of a certain configuration of iron, carbon and hydrogen are thought to be responsible for FT activity. Because these complexes are sparse at the start of FTS, the surface is described to be slowly activated. It is noted here that a fourth, less widely accepted model is sometimes mentioned in the literature. This model considers iron oxide in the form of magnetite (Fe_3O_4) to be an active phase although no detailed description of the active site or reaction mechanism is suggested.[19–22,111]

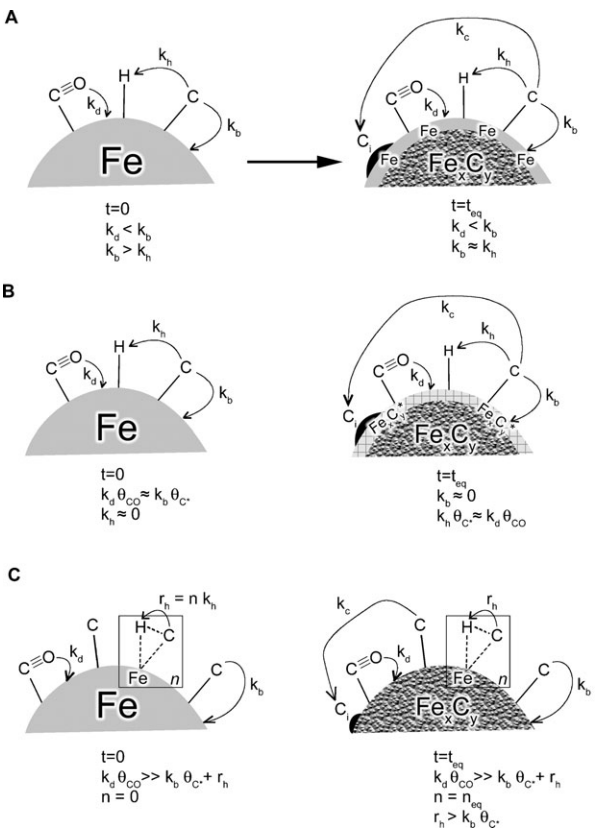

Scheme 1 Proposed models for FTS over Fe-based catalysts: (A) competition model, (B) carbide model and (C) slow activation model.

Proposed reaction mechanisms

Fischer–Tropsch synthesis. The Fischer–Tropsch reaction mechanism has been, and still is, a topic of discussion ever since the first mechanism was proposed in the original paper by Fischer and Tropsch.[134,135] Many detailed reviews are available on the mechanism and models of hydrocarbon and oxygenate formation in FTS.[10,136–146] Because an in-depth discussion of the different reaction mechanisms would be beyond the scope of this review, here we will just give a short overview of the three main mechanisms that have been proposed. In general, all mechanisms presume six elementary reaction steps:[143]

1. Reactant adsorption
2. Chain initiation
3. Chain growth
4. Chain termination
5. Product desorption
6. Readsorption and further reaction

Steps 2 through 4 are, in most cases, accurately described by the Anderson–Schulz–Flory (ASF) kinetics model.[139] This model assumes that the FTS reaction is an ideal polymerisation reaction in which there is one single growth probability factor, α, which determines the hydrocarbon chain length distribution. The model can be described as:

$$m_n = (1 - \alpha)\alpha^{n-1} \qquad (13)$$

α is independent of n and m_n which are the mole fraction of a hydrocarbon with chain length n. α is defined as:

$$\alpha = \frac{R_p}{R_p + R_t} \qquad (14)$$

R_p and R_t are the rates of propagation and termination, respectively. The calculated ASF distribution of several ranges of hydrocarbon chains is plotted in Fig. 5.

The optimal α value for the FTS process depends on the application. As can be seen from the figure, for the production of transportation fuels (C_{12}–C_{18} diesel) the optimal α value is 0.87.

The final elementary reaction step, readsorption, deserves extra attention. Frequently, especially at higher conversions,

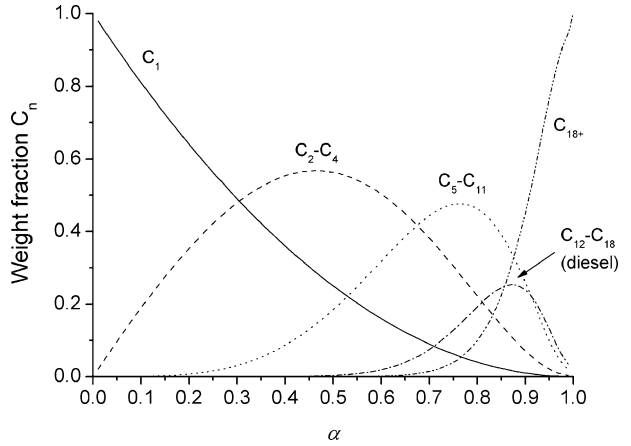

Fig. 5 Weight fraction of hydrocarbon chains of length *n* as a function of the growth probability factor α.

abnormalities are observed in the ASF product distribution as a result of readsorption and reaction of FTS reaction products. These products can be incorporated into other growing hydrocarbon chains on the surface of the catalyst leading to higher weight hydrocarbon chains. Anderson *et al.* calculated that for olefins and alcohols and, to a lesser extent, paraffins, elemental carbon and carbidic carbon this is indeed thermodynamically feasible.[9,139]

Surface carbide mechanism. The first,[134,135] oldest and perhaps most accepted mechanism[91,147] for FTS on iron is the surface carbide mechanism, which proposed chain growth by CH_2 insertion (Scheme 2).[10,148,149] This mechanism presumes dissociative adsorption of CO and H_2, followed by the formation of CH_2 entities which can combine and insert in growing chains. Chain termination can take place either by abstraction or addition of a hydrogen atom from or to the growing chain. It should be noted that in this mechanism, the CH_2 species should be either fixed to the catalyst surface, which implies the need for them to adsorb in close proximity to react; alternatively, it can be assumed that the CH_2 (and CH and CH_3) species are more mobile and are able move over the catalyst surface.[150]

Surface enol mechanism. A second mechanism proposes chain growth through undissociative adsorption of CO (Scheme 3).[9,147,151–153] Surface hydrogen atoms react with the chemisorbed CO groups to form enolic (HCOH) entities. These enolic groups are presumed to either combine through a surface polymerization condensation reaction with loss of water.[9,153] ^{14}C-tracer studies by Emmett and co-workers[154–158] gathered much proof for this mechanism. Or, an alternative option for this mechanism is the individual hydrogenation of the enolic entities, forming water and CH_2 groups[147,151,152] which can grow chains as was described in the previous mechanism.

CO insertion mechanism. The third reaction mechanism involves chain growth through insertion of CO molecules in the metal–carbon bonds (Scheme 4). This mechanism was first proposed in 1958.[159] It was modernized years later by Pichler and Schulz,[160] and further modified by Henrici-Olivé and

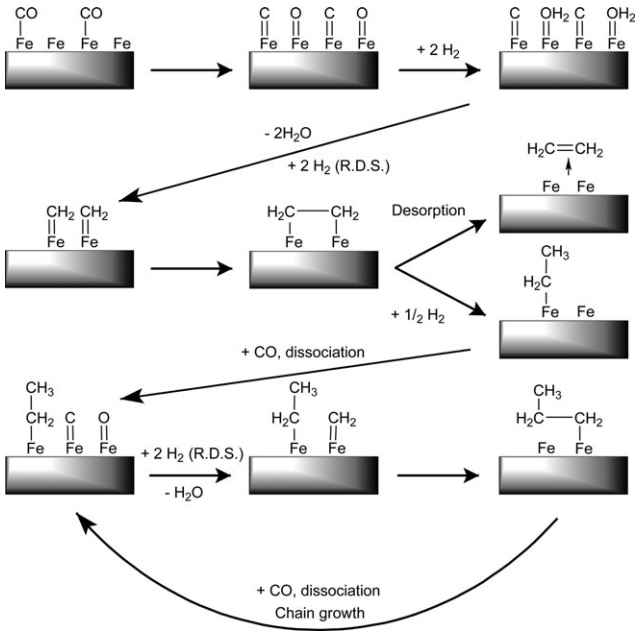

Scheme 2 Representation of the surface carbide mechanism. The rate determining steps (RDS) are indicated in the scheme.

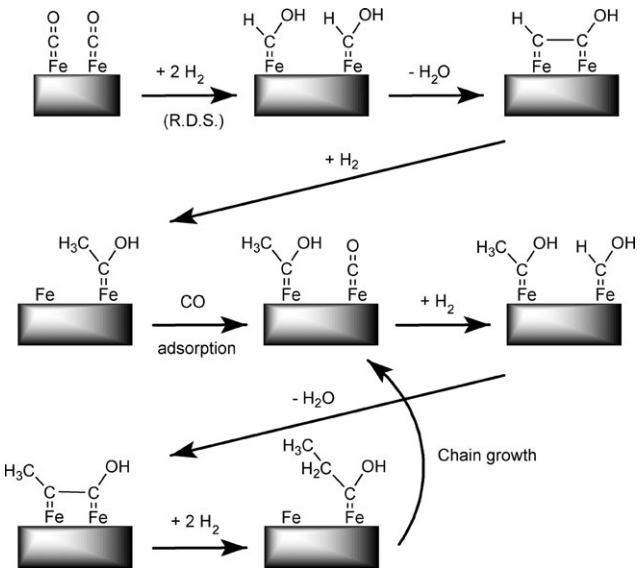

Scheme 3 Representation of the surface enol mechanism. The rate determining step (RDS) is indicated in the scheme.

Olivé,[161] and Masters.[162] The reaction mechanism closely resembles well-known patterns from coordination and organometallic chemistry. A CO molecule is inserted into the metal–H bond in the first (initiation) step. After this, the formed surface aldehyde species is hydrogenated to CH_3 by nearby chemisorbed hydrogen atoms (rate limiting step). Subsequently, CO can be inserted into the metal–carbon bond and the resulting enol species can be hydrogenated again. Chain growth takes place by repeating this step. Termination can take place by hydrogenation of the growing chain, resulting in a free olefin chain and an adsorbed hydrogen atom, from which another chain can initiate.

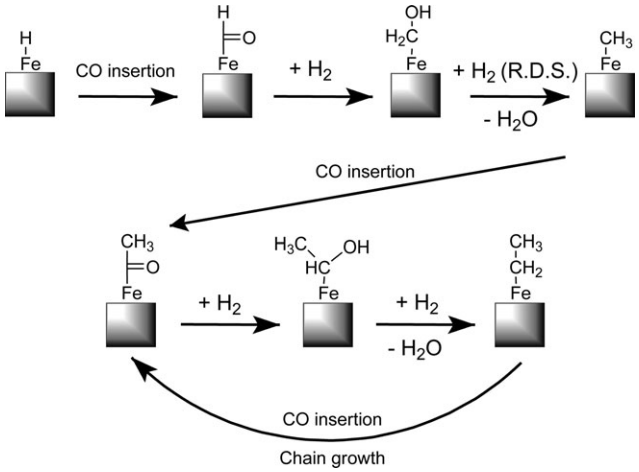

Scheme 4 Representation of the CO insertion mechanism. The rate determining step (RDS) is indicated in the scheme.

Water–gas shift reaction. The mechanism of the catalyzed WGS reaction over Fe_3O_4-based catalysts has been well studied. A typical catalyst is Fe_3O_4/Cr_2O_3 in which the chromium oxide is thought to have no chemical influence on the iron oxide phase. The chromium oxide is mainly added to suppress particle growth during the calcination treatment.[163,164] For similar reasons, sometimes silica is added.[165] Two mechanisms have been proposed in the literature. The first mechanism involves the formation of a surface formate group as CO is inserted into a surface hydroxyl group:[166]

$$* + CO(g) \leftrightarrow CO* \quad (15)$$

$$2* + H_2O \leftrightarrow OH^-* + H^+* \quad (16)$$

$$CO* + OH^-* \leftrightarrow HCOO^-* + * \quad (17)$$

$$*+HCOO^-* \leftrightarrow CO_2* + H^-* \quad (18)$$

$$CO_2* \leftrightarrow CO_2(g) + * \quad (19)$$

$$H^-* + H^+* \leftrightarrow H_2(g) + 2* \quad (20)$$

Experimental support for this mechanism has been given by the observation of a correlation between the amount of surface formate species and the apparent WGS reaction rate.[167] Also, the rate for formic acid decomposition is comparable to that of the WGS reaction further indicating the similarity of the processes.[168] A second, more generally accepted mechanism involves a redox reaction and is named the regenerative mechanism. It is depicted in Scheme 5.

The active site in this mechanism is the anion–cation pair site. More specifically it has been proposed that the octahedrally coordinated iron ions exposed on the catalyst surface are the active sites for WGS.[165] CO coordinates to the iron cations and reacts with the associated surface oxygen atoms to form a bidentate carbonate. Subsequently CO_2 is liberated from the surface, leaving behind a surface oxygen vacancy. On this site, water can be adsorbed, filling the oxygen vacancy and subsequently desorbing H_2. There is ample evidence from chemisorption[165,169] and isotope labeling[170] studies in favor of this mechanism.

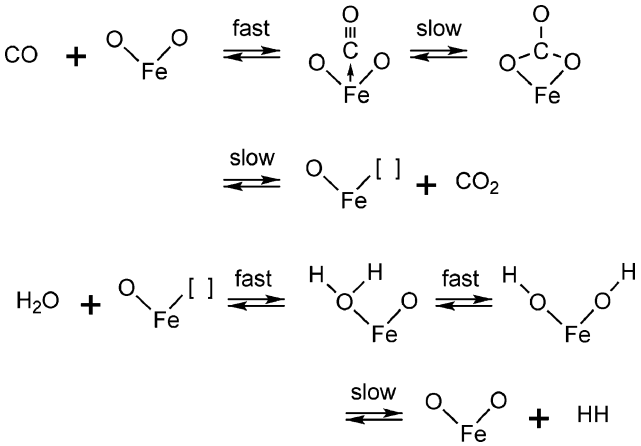

Scheme 5 Suggested "regenerative" mechanism for the water–gas shift reaction.

Catalyst deactivation

There is much debate on the main causes of the eventual loss of catalytic activity for iron-based FTS catalysts. Four main mechanisms of deactivation have been described in the literature:

1. In the first mechanism, it is believed that active iron phases (χ-carbide, ε-carbide, ε′-carbide, more generally Fe_xC or metallic α-Fe) are transformed to catalytically less active or inactive phases. Most groups report that the active phase is gradually oxidized to magnetite (Fe_3O_4), which is inactive in FTS.[1,34,80–84,87–89,104,105,111,171,172] Some groups also consider interconversion of one kind of iron carbide species to another to be a reason for catalyst deactivation. In this case, the intrinsic activity of different iron carbide phases is assumed to be fundamentally different.[43,79,90,102,103,173,174]

2. The second mechanism proposes that deactivation is caused by the deposition of inactive carbonaceous compounds (*e.g.* graphitic carbon, amorphous carbon, coke) on the surface of the catalyst, thereby limiting the contact between reactant gases and the catalytically active phase.[20,22,40,42,70,78,81,83,84,91–93,112–114,173–180]

3. Thirdly, some groups report that sintering, the loss of catalytic surface area due to ripening or migration and coalescence of the iron phase, is a main cause for the loss of activity.[1,10,80,87,90]

4. Finally, iron-based catalysts are reported to be poisoned and deactivated by sulfur compounds, present in (most) industrial syngas feeds.[1,10,75,80,83,87,107,181–183]

While in some research a single mechanism is believed to be responsible for the deactivation of the catalysts, most groups propose that the catalysts deactivate due to the contributions of more than one mechanism. Scheme 6 shows a simplified sketch of the different deactivation mechanisms of a pre-reduced iron catalyst. These deactivation pathways will be briefly addressed below.

Deactivation through phase changes. The reducibility of metal oxides increases from Fe, Co, Ni to Ru. It can therefore be expected that the reoxidation of the metallic phases decreases in the same order. It has indeed been well documented indeed that, for iron, Fe_3O_4 is found during FTS, while for Co,

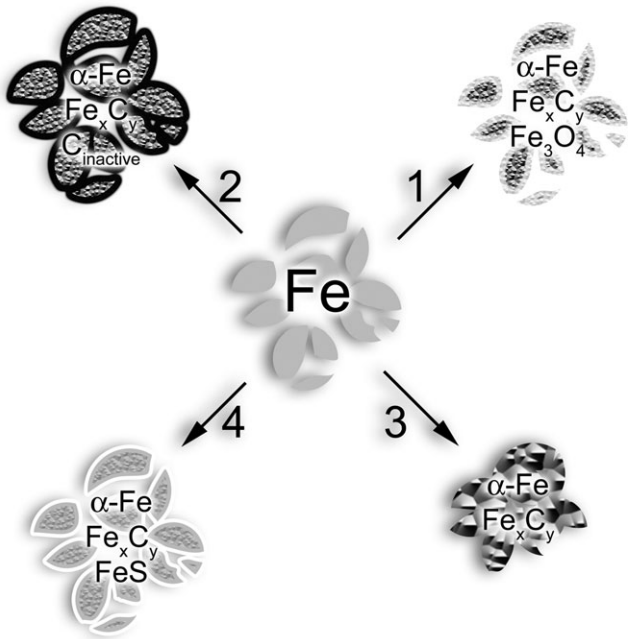

Scheme 6 The four deactivation pathways in Fe-based Fischer–Tropsch catalysts.

Ni and Ru no oxides are formed.[75] Fig. 6 illustrates the change in bulk composition of a pre-reduced iron catalyst during FTS.

Deactivation by oxidation can be described by the reverse reactions of those sketched out above (eqn (7) and (8)):

$$xFe + yH_2O \leftrightarrow Fe_xO_y + yH_2 \quad (21)$$

$$xFe + yCO_2 \leftrightarrow Fe_xO_y + yCO \quad (22)$$

When these reverse reactions are combined with the reactions for carbide formation we get:

$$Fe_xC_y + yH_2O \leftrightarrow yC^* + yH_2 + Fe_xO_y \ (21 + 10)$$

$$Fe_xC_y + yCO_2 \leftrightarrow yC^* + yCO + Fe_xO_y \ (22 + 10)$$

The above reactions sum up one of the main proposed mechanisms of deactivation of iron-based catalysts during FTS: oxidation of the active phase. According to Dry,[142]

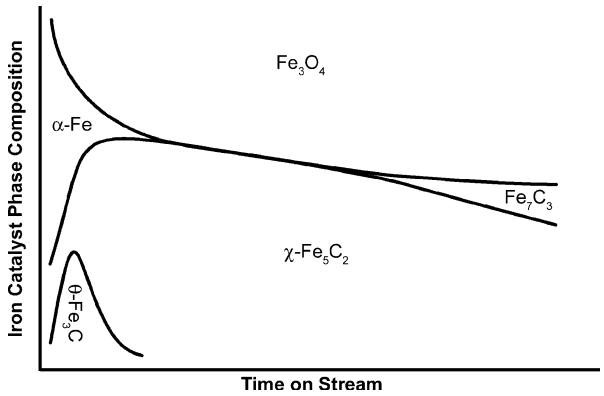

Fig. 6 Bulk composition changes of a pre-reduced iron catalyst during Fischer–Tropsch synthesis (reproduced from ref. 10).

the kinetics of the FTS reaction over iron can be described as:

$$r = \frac{mP_{CO} \cdot P_{H_2}}{P_{CO} + aP_{H_2O}} \quad (23)$$

where a is the ratio of the H_2O and H_2 adsorption constants (k_{H_2O} and k_{H_2}).

Water vapor, which is one of the main reaction products in the FTS reaction, has a negative reaction order in the rate equation and as a result the reaction rate drops as the partial pressure of water becomes higher in the reaction. As water production is directly coupled to carbon dioxide production through the WGS reaction, the same holds for carbon dioxide. As in catalyst beds increasingly more reactant gas is converted and thus more water and carbon dioxide reaction products are present upon moving from the bed entrance to the exit; this implies that oxidation of the active phase becomes a bigger problem upon moving further into the catalyst bed.[87] Iron carbides are considerable more resistant to oxidation by water than metallic iron. Interestingly, it has been observed that smaller catalyst particles carburize more rapidly and are not oxidized during reaction while larger particles showed higher oxide : carbide ratios.[10,42] This observation is explained by the fact that the synthesis gas mixture not only becomes more oxidizing upon moving down the catalyst bed, but also upon moving further down the catalyst pores. On a smaller scale, the gas mixture can become very oxidizing (high H_2O and CO_2 partial pressures), leading to the oxidation of the cores of catalyst particles. Indeed, it was observed that for certain iron oxide catalysts[1,75,184] the activity did not increase beyond a reduction extent of about 30%. The model of catalyst particles with an iron oxide Fe_3O_4 core and iron carbide shell has been widely applied since.

Another related deactivation mechanism which is sometimes found in the literature proposes that catalysts deactivate because the active iron carbide phase is gradually transformed into a less (or non) active iron carbide phase:

$$Fe_xC_y \rightarrow Fe_xC_{y-z} + zC^* \quad (24)$$

Deactivation through deposition of inactive carbonaceous compounds. Active surface sites of a FTS catalyst can be "fouled" and become blocked by different kinds of surface poisons. Under typical FTS operation conditions, both (liquid) high molecular weight waxes and insoluble carbonaceous compounds are formed and are able to drastically lower catalyst activity over time. However, while high molecular weight waxes partially fill the catalyst pore and thereby retard the rate of diffusion of reactants, insoluble carbonaceous deposits permanently block active surface sites leading to lower activity and higher methane selectivity.

A common way to describe the deposition of insoluble carbonaceous compounds (Boudouard) during reaction is:

$$C^* + 2CO \rightarrow C\text{–}C^* + CO_2 \quad (25)$$

$$C^* + CO + H_2 \rightarrow C\text{–}C^* + H_2O \quad (26)$$

At low temperature Fischer–Tropsch (LTFT) reaction temperatures (<280 °C), mainly amorphous carbon is deposited. At higher reaction temperatures (>280 °C), graphitic carbon formation becomes more and more favorable, leading to coke deposition. Several studies have focused on the characterization of inactive carbon species formed during FTS.[40,77,78,83,88,106,114,120] The thus formed compounds (amorphous and especially coke) are very sparsely removed from the catalyst surface during reaction. Hydrogen treatments at elevated temperatures (>350 °C) are commonly used to reactivate catalysts. Several patented methods[185–187] are described in the literature. Alternatively, steam assisted catalyst regeneration has been reported as well.[188] The amount of carbon fouling is very dependent on the pretreatment conditions of the catalysts. Pre-reduced catalysts for example are known to be more prone to carbon fouling compared to fully carburized catalysts.

Deactivation through sintering of the active phase. All iron-based FTS catalysts to some extent suffer from deactivation by sintering of the active phase. Traditionally, sintering can be described as the process of the growth of small crystallites due to ripening or migration and coalescence phenomena. An important value to consider with respect to sintering is the Tamman temperature. This value is defined as half of the bulk melting point (in K). Above these temperatures, atoms on the surface of crystallites are expected to become mobile and as a result crystallites can sinter.[189] The Tamman temperature for iron is 906 K (633 °C). This is much higher than typical temperatures used for FTS (200–300 °C). It is, however, possible that the local temperature of crystallites is much higher, due to the heat that is released in the strongly exothermic FTS reaction. Typical "as prepared" iron oxide catalysts characterized by N_2 physisorption have a BET (Brunauer–Emmett–Teller) surface area of around 100–300 m^2. After reduction and carburization (and passivation) it is often observed that the BET area decreases to about 10–90 m^2.[10,84,140,190] However, it remains difficult to prove that sintering is a main pathway of deactivation during FTS. Although some have reported hydrothermal sintering, as a result of high partial pressures of H_2O in the catalyst bed, as a cause for catalyst deactivation.[10,87] Catalyst particles are often reported to break up[90,98,105,191] by deposition of carbon or attrition during FTS, resulting in the exposure of more active sites rather than less. Also, detecting catalyst sintering from BET surface areas alone can be complicated as surface areas are often found to increase during time on stream because of the deposition of carbon.[192] However, it is well known that by adding some SiO_2, Al_2O_3, ZnO or other support as a binder catalysts typically show lower deactivation rates. This is generally ascribed to the prevention of sintering by the stabilization of the active phase by the binder material.[193–195] Typically, this positive effect has not been reported when the same materials are used in slurry bubble-column reactors.[193]

Deactivation through poisoning. In general, catalyst deactivation by chemical poisons is reported and studied more commonly in the context of industrial catalysis than in academia. Well-known poisons are electronegative elements like oxygen, chlorine, bromine and sulfur. Especially the effect of sulfur on the properties of iron FT catalysts has been studied in much detail. Both poisoning effects as well as promotion are reported in the literature.[10,62,80,83,87,107,181–183,196–201] If present in high concentrations (~10 ppm), sulfur decreases catalyst activity while not directly affecting the selectivity. At lower concentrations (~0.5 ppm), sulfur is reported to increase the catalyst reducibility[62,196] and improve the olefin selectivity.[197–201] A review of the effect of sulfur is given by Madon and Shaw.[61]

In most industrial gas feeds, sulfur compounds are present that can rapidly deactivate iron[1,10,75,80,83,87,107,181–183] (as well as cobalt and nickel) catalysts. The most common sulfur poison is H_2S. CH_3SH,[1] C_2H_5SH[10] and COS[75,107] are often reported as well. It has been reported that organic sulfides can penetrate deeper into catalyst beds, thereby poisoning a larger portion of the catalyst.[1,10] Fischer himself realized the poisonous effect of sulfur on the FT catalysts and recommended an upper operation limit of 1 to 2 mg m^{-3} of sulfur in the synthesis gas feed.[202] However, as Dry noted,[10] to assure minimal poisoning the sulfur content should be about ten times lower than this value. Sulfur poisoning is a significant problem for industrial FTS plants; especially since sulfur poisoned catalysts are not readily reactivated. Sulfur poisoned catalysts treated in a high temperature reduction step in hydrogen show no reactivation. In fact, hydrogen reduction has been reported to lower the catalyst activity even more, as a result of a redistribution of the sulfur over the catalyst bed.[75] The only reported way to reactivate the catalysts is a high temperature re-oxidation step to burn away the adsorbed sulfur compounds.[10,75]

Deactivation

As was described above, iron-based FTS catalysts can lose their activity over time (deactivate) due to several different reasons:

1. The conversion of the active phase (metal, carbide, *etc.*) to an inert phase (oxide, different carbide phase).
2. The loss of active surface area due to the deposition of carbonaceous material ("fouling").
3. The loss of active surface area due to crystalline growth (sintering).
4. The chemical poisoning of the surface (*e.g.* by sulfur).

In the following, the different deactivation mechanisms and the influence of the pretreatment conditions on these mechanisms will be described in more detail against a background of open literature.

Deactivation through phase changes

Deactivation by oxidation of the active iron(carbide) phase. In their studies of the spent precipitated iron catalyst from a pilot plant,[80,87] Duvenhage *et al.* found two main causes for catalyst deactivation. Using SEM-EDX (scanning electron microscopy-energy dispersive X-ray analysis), SIMS and XRD it was shown that near the top of the catalyst bed, the catalyst was poisoned by sulfur present in the reactant feed. Near the middle and bottom part of the catalyst bed, the catalyst deactivated due to sintering and oxidation of iron (carbide) species to Fe_3O_4. The authors attributed both sintering and

oxidation of the catalyst to the reaction with H_2O and CO_2 formed by the WGS reaction. As a result of this reaction, the gas feed mixture becomes more oxidizing in nature going down the catalyst bed, resulting in faster deactivation near the bottom of the catalyst bed.

In their research on the activation of a doubly promoted precipitated iron-based FTS catalysts (100Fe : 0.3Cu : 0.8K), Bukur *et al.* found that the activity of their catalyst decreased with time on stream if it was pretreated by carbon monoxide or syngas.[81,83,84] In contradiction with many other papers, their H_2 reduced catalysts did not show any deactivation, even at very long times on stream (150+ h). This was explained by the hypothesis that the higher surface concentration of hydrogen on these catalysts somehow stabilized catalyst activity. The H_2 reduced catalyst did show higher selectivity toward methane, lower hydrocarbons, isomers and olefins as compared to the CO and syngas pretreated samples. The deactivation of the CO and H_2–CO pretreated catalysts was attributed to the conversion of the FT active χ-Fe_5C_2 species to a less active iron oxide phase and the buildup of carbonaceous species on the catalyst surface. The characterization of the used catalyst by Mössbauer spectroscopy and XRD showed that the χ-Fe_5C_2, the dominant phase after carbon monoxide and syngas pretreatments (84–95%) was largely converted to magnetite, ε'-$Fe_{2.2}C$ and siderite ($Fe(CO_3)$). The group proposed that χ-Fe_5C_2 might be oxidized to magnetite in the oxidizing atmosphere near the reactor outlet (similar to observations by Duvenhage *et al.*[80,87]) after which it can be carburized to ε'-$Fe_{2.2}C$, which appeared to be more resistant toward oxidizing conditions. The formation of the siderite phase was linked to the production of carbon dioxide in the water–gas shift reaction.

Dry,[1] Gormley *et al.*,[105] Bartholomew *et al.*,[171] and Ning *et al.*[88] all also reported the partial pressure of H_2O and CO_2 produced from the WGS reaction to be responsible for the oxidation and/or sintering of the catalyst. Dry reported that in industrial catalysts used by Sasol main contributors to catalyst deactivation are sulfur poisoning, coke laydown, hydrothermal sintering and oxidation.[1] Gormley *et al.* found that when they were using a heavier initial wax reaction medium in their slurry reactor the catalyst deactivated more rapidly.[105] It was suggested that the heavier waxes might restrict the diffusion of water vapor formed by the WGS reaction out of the catalyst pores, leading to local high partial pressures of water which could irreversibly oxidize the catalyst. Bartholomew *et al.* reported that the χ-carbide, the only active phase found in their catalyst, was oxidized more rapidly at higher pressures of CO_2 and H_2O.[171] The group also found that higher temperatures led to faster oxidation of the carbide while the addition of silica slowed down the oxidation process.

Ning *et al.* also supported the mechanism of water vapor as a main cause of the deactivation of precipitated iron-based FTS catalysts by oxidation of the iron carbide phase (χ-Fe_5C_2 and Fe_xC).[88] Their observations from XRD analysis matched the observations of other groups that the oxidation of the catalyst near the reactor outlet was more pronounced. Using RS, the group did not find any proof for the formation of carbonaceous compounds during FTS. The authors therefore claimed it was unlikely that the deactivation of the catalyst is caused by deposition of inactive carbonaceous layers, as claimed by other groups.[20,22,40,42,70,78,81,83,84,91,93,112–114,173–177]

In an extensive structural characterization study using XAS and MES, Li *et al.*[34] found that the deactivation of their precipitated iron catalyst (pre-reduced in CO) in the FTS reaction, paralleled the conversion of iron carbides to magnetite.[34] The group found that after 450 h of reaction time, magnetite was the only iron phase present in the catalysts. However, different from the proposed oxidation mechanism of the aforementioned groups,[80–81,83,84,87,88,105,171] Li *et al.* offered an alternative explanation for the oxidation of the active iron phase. Based on their research the authors suggested that changes at the carbide surface lead to a higher susceptibility for carbide oxidation. The replenishing of carbidic surface sites and the removal of chemisorbed oxygen is thought to be selectively inhibited. As a result, the active iron carbide phase is oxidized, even in the presence of a reducing gas mixture.

Mahajan *et al.*[111] also performed a combined XAS-MES study focusing on three iron catalysts, two unsupported and one supported. The catalysts were pre-reduced (carburized) in CO for 24 h. Similar to Li *et al.*, characterization of the quenched catalysts showed that after 120 h the catalysts were largely converted to magnetite (60–80%), with the remainder of the iron being present as iron carbides. In their case however, catalyst activity appeared to be very stable. It is striking that in this case the appearance of magnetite phase is not correlated to any apparent deactivation of the iron catalyst. The authors even suggested the magnetite phase to be catalytically active.

Further support for the deactivation-by-oxidation mechanism is given by Raje *et al.*,[172] Zhang *et al.*,[104] and Hayakawa *et al.*[89] Raje *et al.* confirmed that catalyst with and without added silica and potassium promoter species deactivated and consisted of mainly iron oxide after reaction.[172] A catalyst solely promoted with potassium consisted of iron carbides after prolonged reaction times. The group found that the partial pressure of water in the catalysts which contained potassium was significantly lower. However, because the silica and potassium promoted catalyst deactivated in time while the catalyst containing only potassium remained active, the group concluded that the influence of water on the deactivation mechanism was not clear. Zhang *et al.* correlated the deactivation of precipitated iron catalysts with the transition of iron carbide phases (χ-carbide or $Fe_{2+}C$) to magnetite.[104] The authors showed that for unpromoted catalysts, the χ-carbide phase present after activation was gradually transformed into 100% magnetite after 450 h FTS. In contrast, a potassium promoted catalyst was shown to remain in a $Fe_{2+}C$ phase even after 400 h on stream. Without suggesting a mechanism, the group concluded that both carbide phases are comparable in activity in FTS while the χ-carbide is more susceptible to oxidation over time.

Finally, more support for the oxidation mechanism came from Hayakawa *et al.*, who recently published a paper on a XRD and TPR study of precipitated iron catalysts.[89] The group concluded that the relative quantity of χ-carbide to magnetite correlated with the activity of the catalyst and the formation of more magnetite led to lower catalyst activity.

Deactivation by interconversion of carbide species. In this section, catalyst deactivation with interconversion between different carbide species as the main mechanism will be discussed. Some research groups refrain from describing the exact chemical identity of carbide phases that are interconverted.[102,103] This makes it sometimes hard to determine if the mechanisms of deactivation are inherently different from deactivation by deposition of carbonaceous compounds as described above. Fortunately, other groups do distinguish between the different crystal structures (ε, χ, θ, *etc.*) of the iron carbides formed as FTS proceeds.[43,79,90,173,174]

In two papers, Lazar and co-workers describe the deactivation of iron catalysts using *in situ* MES along with kinetic measurements. In the first paper,[103] the group reports the progressive conversion of FTS active mobile carbide species into immobile carbide species which are mainly selective toward methane production and finally to bulk, inactive χ-Fe_5C_2 carbide species. Unfortunately, no suggestions are made on the exact identity and composition of the active carbide species. The second paper[102] deals with the effects of promoter elements and support materials on the stabilization of small iron particles and the deactivation kinetics of the catalysts. The group observed that smaller iron particles are less susceptible to deactivation. From MES measurements it was observed that smaller particles were never fully reduced to metallic iron. The Fe_3O_4 phase that was formed after reduction of the small particles hardly changed during FT reaction and the catalyst showed no apparent signs of deactivation. This result agrees with the results found by Dictor and Bell,[91] even though the groups suggest different mechanisms of deactivation.

The work by Eliason and Bartholomew,[173,174] besides the formation of graphitic layers, also considers the interconversion of carbides as a pathway for catalyst deactivation. On the basis of observations in other papers, the group proposed that iron catalysts deactivate by parallel formation of polymeric carbon deposits and conversion of the FTS active, carbon rich, ε′-$Fe_{2.2}C$ phase to the χ-Fe_5C_2 and subsequently to the θ-Fe_3C. Unfortunately, no direct evidence for this mechanism is presented in the paper to back up the results.

In a paper that deals with the deactivation of FTS catalysts by interconversion of carbide species, Pijolat *et al.*[43] used MES and IR to attempt to elucidate the deactivation of a Fe/Al_2O_3 catalyst. The paper describes two different contributions to the deactivation of their catalyst. Firstly, the fast (within a few minutes) deactivation as the catalyst is exposed to syngas is attributed to the coverage of the metallic iron surface by a layer of carbonaceous deposits (in accordance with other groups[20,22,40,42,70,78,81,83,84,91,93,112–114,173–177]). For the decrease in activity during longer times on stream, two hypotheses are proposed:

1. The covering of the remaining active iron sites by carbonaceous deposits.

2. The progressive take up of carbon of a surface carbide species $Fe_{2+x}C$ (decreasing x) thereby causing a decrease in catalyst activity.

From IR, no CO was found to adsorb onto metallic sites of the catalyst after a few hours of reaction. Because the catalyst was still active during this time, the authors ruled out hypothesis 1. By combining their Mössbauer results on the iron carbide composition and catalytic testing, the group found that the activity in the FTS reaction actually scaled linearly to the stoichiometry of the $Fe_{2+x}C$ phase present in their catalysts, thus presenting evidence for a deactivation mechanism by interconversion of iron carbides.

Deactivation through deposition of inactive carbonaceous compounds

Dry *et al.* studied the factors influencing the deposition of free carbon on the catalyst surface.[179,180] Although there is no discussion about the exact effect of the carbon deposition on the deactivation of the catalysts, it might be interesting to shortly consider the results. The first paper[179] considers the influence of Lewis basic (electron donating) promoters on the rate of the Boudouard reaction (eqn (25) and (26)). The authors found that the addition of basic promoters like Na_2O and K_2O had a positive influence on the rate of formation of free carbon. The more basic K had a higher promotional effect on this rate. Structural promoters, such as SiO_2, Al_2O_3 and CaO, had no significant influence on the intrinsic (corrected for the total iron surface area) rate of carbon formation, although the most basic CaO support showed a little higher rate. By combining the basic promoters with structural promoters it was found that the total electron donating potential of the basic promoters was reduced leading to somewhat lower carbon deposition rates per unit iron area. The second paper[180] assessed the influence of the reaction temperature and gases and vapors on the rate of carbon deposition. Here the authors found that upon increasing the reaction temperature from 285 °C to 338 °C the rate for carbon deposition increased tenfold, illustrating the strong temperature sensitivity often reported by other authors for deactivation by carbon fouling. Water vapor, hydrogen, aliphatic acids, alcohols and ketones, all potentially present in the gas phase during FTS, were found to enhance the carbon deposition rate. This was rationalized by assuming that water, aliphatic acids, alcohols and ketones all decomposed to form molecular hydrogen. The hydrogen could enhance the CO adsorption potential by either reducing the iron carbide phase to metallic iron or by the more subtle process of mutual enhancement of adsorption. In this process, hydrogen acts as an electron donor to the iron surface, enhancing the metal to carbon bond and weakening the carbon to oxygen bond in adsorbed CO. When the results by Dry *et al.* are viewed in the light of carbon fouling and catalyst deactivation, one could at least partially explain why alkali promoted catalysts often show higher deactivation rates, why structurally promoted catalysts are more stable for longer reaction times and why higher reaction temperatures lead to the deposition of more inactive carbon on the catalyst surface. The influence of higher partial hydrogen pressures on the deactivation of catalysts is less well documented in the literature and therefore this effect cannot be readily rationalized.

Niemantsverdriet *et al.*, studied the behaviour of metallic iron catalysts during FTS.[70] Using XRD and MES they found four different iron carbide phases present during FTS: θ-Fe_3C, χ-Fe_5C_2, ε′-$Fe_{2.2}C$, Fe_xC. However, from carbon content

analysis it was determined that after 6.5 h reaction time, significantly more carbon was present in the catalyst than calculated on the basis of the iron carbide structures predicted by MES and XRD. Because it was also found that the iron catalyst started to deactivate within this time frame, their conclusion was that deactivation was mainly caused by the formation of excessive amounts of inactive carbon on the surface of the catalyst.

Dwyer and Somorjai studied the hydrogenation of CO and CO_2 over iron foils.[114] They showed with Auger spectroscopy that after about 4 h of reaction time, the surface of the foils was completely covered with carbonaceous species. After this reaction time the only product that was formed was methane, at a very low rate relative to the initial activity. They suggested that the iron carbide phases present during the hydrogenation reaction can either be hydrogenated or catalytically reduced, with the latter responsible for formation of carbonaceous over layers and the subsequent loss of activity. From eqn (25) and (26) it is clear that high partial pressures of H_2O and CO_2 should inhibit the formation of Boudouard type carbonaceous compounds and thereby slow down the deactivation of the iron foil. This is very different from the conclusions described in the previous paragraph, where high partial pressures of H_2O and CO_2 were predicted to deactivate the iron catalysts. Noting the difference in deactivation rates between iron foils and precipitated iron catalysts, Dwyer and Hardenbergh later investigated and compared the reduction of CO over low surface area iron (foils) and high surface area iron powders with XPS and catalytic tests.[112] They found that powders were less susceptible to the formation of graphite, although they were eventually poisoned by graphite at temperatures above 275 °C.

In a series of papers, Raupp and Delgass[42,92,93] reported on the phase composition of iron FTS catalysts supported on SiO_2 and MgO. Using MES it was shown that during FTS a bulk iron carbide (χ-Fe_5C_2) phase is gradually formed. The authors describe a competition between the formation of surface and bulk carbide species, much like the competition model later described by Niemantsverdriet *et al.*[70] The formation of the bulk carbide phase was almost complete after 6 h of reaction time for the SiO_2 supported catalyst and 3 h for the MgO supported catalyst. Within the first 40 min, however, mainly ε-Fe_2C and ε'-$Fe_{2.2}C$ species were observed. Interestingly, hardly any deactivation was observed after the formation of the bulk carbide phase was complete. The activity steadily rose to a maximum as the bulk phase was formed. This disagrees with the mechanism of deactivation by interconversion of carbide species. Although no direct evidence is presented, the deactivation that was observed after longer reaction times was ascribed to the formation of carbonaceous deposits on the surface of the catalysts. By flowing hydrogen over the carburized catalysts at 523 K, the group further found that only methane was formed from the hydrogenation of the iron carbides. In addition they found that although surface carbide species were hydrogenated relatively fast, bulk carbides were hard to hydrogenate, illustrating that carbon migration from the bulk to the surface is a slow process.

Krebs *et al.* also investigated the hydrogenation of CO over iron foils in a series of papers.[40,113,175] Their group used AES and XPS along with catalytic tests to study the phases responsible for the deactivation of the foil. The main conclusion of their research was that the hydrogenation activity of the iron foil decreased faster at higher temperatures and larger $CO : H_2$ ratios. Two forms of carbon could be distinguished on the surface of the foil: carbidic carbon and graphitic carbon. The carbidic carbon could be hydrogenated readily, while the graphitic carbon could not. As was the case in the research of Dwyer and Somorjai,[114] the formation of graphitic carbon coincided with a decrease in hydrogenation activity. Therefore, the deactivation of the foil was attributed to the growth of carbonaceous overlayers. In addition it was shown that the deposition of a potassium layer on the iron foil led to lower methanation rates and higher rates of graphite deposition.[175]

In a study on the surface structure of reduced and unreduced Fe_2O_3 during reaction with H_2 and CO, Reymond *et al.* used XRD and XPS to show that inactive carbon is responsible for catalyst deactivation.[20] It was observed that a pre-reduced sample (α-Fe) was more susceptible to deactivation. In this catalyst, $Fe_{20}C_9$ was found to be an inactive phase of the iron catalyst by XRD, while for the unreduced (Fe_2O_3) catalyst this was ε-Fe_2C. From the observation that the formation of magnetite (Fe_3O_4) parallels the onset of FTS activity, the authors also suggest that magnetite might be an active phase in the iron based catalysts. Carbide formation was faster when the catalysts were exposed to a $CO–H_2$ (1 : 9) mixture for the pre-reduced sample while the rate of consumption of the carbides was found to be much slower when the catalysts were exposed to pure H_2 after FTS reaction. Therefore it was concluded that inactive carbonaceous species are responsible for the deactivation of the iron catalyst.

Dictor and Bell, in a similar methodology, studied FTS over reduced and unreduced iron oxide catalysts.[91] Here, high initial activity but subsequent rapid deactivation of the pre-reduced catalyst is reported. In contrast, the unreduced catalyst exhibits much lower rates of deactivation. Although similar to the study by Reymond *et al.*,[20] no direct evidence of unreactive carbonaceous species is given, the authors suggest that the catalyst deactivates in time by accumulation of these species. XRD analysis shows the presence of ε'-$Fe_{2.2}C$ in both the unreduced and reduced catalyst but in the case of the latter a larger quantity of the carbide is observed. However, because the reduced catalyst showed less FTS activity, the authors suggest that the ε'-$Fe_{2.2}C$ crystallite size is smaller in the case of the (more active) unreduced catalyst. The smaller sizes of these crystallites are also deemed responsible for the lower activation rates in this catalyst. It must be noted however that no evidence for smaller carbide particle sizes was found in the XRD patterns (*e.g.* no observed line broadening). Also, it was not noted that, since the XRD patterns were recorded after reaction and not *in situ*, the lower abundance of carbides on the more active catalysts might be due to the fact that the carbides are oxidized more rapidly in this case.

Sommen *et al.*, reported the deactivation of carbon-supported iron catalysts for production of C_2 and C_3 olefins from syngas.[176] They found that high levels of CO_2 were produced, mainly due to the Boudouard reaction. It was estimated that only 20% of the converted CO produced hydrocarbons. In their catalytic system, carbon deposit

formation exceeded hydrocarbon formation by a factor of 2. Using thermobalance measurements the group illustrated that the catalyst weight in certain cases increased by 30% under syngas feed. This high increase cannot be explained by the formation of iron carbide species and thus must be due to the formation of inactive carbon deposits. In this respect, the group observed growing (graphitic) carbon fibers in their TEM analysis. Unlike other authors however, Sommen *et al.* did not ascribe the deactivation of the catalyst to the coverage of active iron sites, but rather to the blockage of catalyst pores leading to a lower amount of accessible iron. Their main argument for this was the high initial deactivation rate, which cannot be explained by the simple progressive deposition of carbon on active iron surfaces.

McDonald *et al.*[178] studied the influence of the iron particle size for a Fe/MgO catalyst. They found that smaller particles were less active for methane production but showed a higher C_{2+} selectivity and deactivated less with reaction time. The lower tendency to deactivate was ascribed, at least partly, to the lower amounts of inactive surface carbonaceous species present on the smaller particles. This was thought to be due to the higher extent of carburization of the smaller iron particles, leading to lower CO dissociation rates. Similar to Raupp and Delgass[42] and Jung *et al.*,[203] the group found that smaller iron particles showed a preference to form the ε'-$Fe_{2.2}C$ phase over the χ-Fe_5C_2 phase. Jung *et al.* concluded similarly from their experiments on highly dispersive iron catalysts supported on carbon and alumina.[203] The highly dispersed catalysts showed a superior maintenance in activity. The group stated that, because of the first order dependence of the FTS reaction rate in hydrogen[204] and the fact that smaller iron particles show lower hydrogen chemisorption potential, the overall reaction rate over smaller particles is expected to be lower. Therefore, it might be expected that less carbonaceous deposits are formed on these catalysts.

Bukur *et al.*[81,83,84] observed the deposition of carbon during the activation treatment as well as during FT synthesis. It was observed that under FTS conditions, except for the aforementioned oxidation to Fe_3O_4, the χ-Fe_5C_2 phase was gradually converted into inactive carbon deposits. The authors commented that the catalysts containing some amount of binder deactivated much slower. This is ascribed mainly to the reduced extent of masking of active sites by carbonaceous deposits. The authors confirm that some sintering also contributes to the overall deactivation of the catalyst. Like Sommen *et al.*,[176] Machocki[78] applied TGA measurements in his research into the deactivation of silica-supported Fe catalysts (15 wt%) at 275 °C and 1 bar. His work nicely fits the proposed competition model as described by Niemantsverdriet *et al.*[70] During time on stream, rapid weight increase during the activation period as syngas is first introduced to the reduced catalyst, weight decrease as the catalyst reaches it maximum activity and subsequent weight increase as the catalyst deactivates are all observed. Because the maximum theoretical weight increase (relative to the total iron mass) from iron carbide formation (Fe_2C) is 9.709 wt%, the additional mass increase can only be explained by the binding of oxygen originating from dissociated carbon monoxide species. This implies that, apart from iron carbide, also some iron oxide species are formed. The weight increase after longer times on stream is due to the deposition of unstoichiometric amounts of carbon on the surface of the catalyst. From XRD after 50 h on stream, the author found that except for the amorphous carbon deposits, the only phases that were present were χ-Fe_5C_2 and Fe_3O_4.

Shroff *et al.*[132] specifically studied the role of different iron phases during FTS. From their research the group concluded that the iron carbide phase is necessary for the catalyst to show FTS activity. Using HRTEM, XRD and XPS/AES, the group observed the conversion of iron oxide into smaller iron carbide particles after activation in CO and syngas mixtures. After prolonged FTS reaction time, carbon layers were observed on the surface of the iron carbide particles. Similar to what is proposed by other groups, Shroff *et al.* assumed that the catalyst deactivated by the inhibition, or rather physical covering, of the reactive surface of the catalyst by carbonaceous species.

Eliason and Bartholomew[173,174] proposed that the iron catalyst deactivation is caused by parallel paths, *i.e.* (a) the conversion of atomic carbon to polymeric and graphitic carbon and (b) the interconversion between active and less active iron carbides. Although the authors do not present any direct proof for the formation of these species, a mechanism is proposed for the deactivation of the catalyst. This mechanism involves the formation of polymeric, graphitic and carbidic carbon.

Finally, we would like to include a study on the hydrogenation of CO_2 on a Fe-K/Al_2O_3 catalyst by Hwang *et al.*[177] It is included in this discussion because this reaction is closely related to the Fischer–Tropsch reaction, as CO_2 is actually converted to CO before hydrogenation. In this research it was shown by chemisorption, BET analysis and XRD that carbonaceous deposits were formed after prolonged reaction time and, interestingly, that the catalyst could be regenerated by an oxidation–reduction treatment.

Deactivation through sintering of the active phase

Sintering has been reported to be a cause for catalyst deactivation by various authors.[1,80,87,90] Dry[1] reported that the BET area and the amount of pores with sizes below 35 nm of aged catalysts declined while the crystallite size increased upon moving down the (fixed) catalyst bed. This indicates sintering of the catalytic phase. In addition, the catalyst bed had more oxidic character in the lower part of the reactor. Therefore it was assumed that hydrothermal sintering and oxidation were the main causes for the catalyst deactivation in the bottom part of the catalyst bed. The progressively increasing H_2O partial pressure upon going down the catalyst bed was the main reason for the increased amount of sintering. Duvenhage *et al.*[80,87] drew similar conclusions in their research on industrial FT catalysts.

Mansker *et al.*[90] also reported sintering in their study of a precipitated FTS catalyst material. The researchers found that the change in carbide phase composition from Fe_7C_3 to χ-Fe_5C_2 was accompanied by a progressive growth in crystallite size after ~350 h on stream. However, it was unclear whether the deactivation was directly related to the sintering of

the carbide phase or that the carbide phases were inherently different in activity.

Sintering in iron FTS catalysts remains a very delicate subject. The phase changes that the catalyst undergoes have great impact on the surface area of the catalyst. In this respect sintering is often reported in the context of reduction,[19,79,81,108,175,205] rather than during the FTS reaction. During reduction, the porous structure of the iron oxide precursor is lost as metallic iron sinters, resulting in a drop in surface area and total pore volume. To prevent this, very often transition metal catalysts are directly converted to carbides without a separate reduction step.[46] As iron carbides have substantially higher melting points (θ-Fe_3C $m_p \approx 2100$ K), and thus higher Tamman temperatures, than metallic iron ($m_p \approx 1811$ K), the extent of sintering is expected to be significantly lower for carbides as compared to iron. For iron FTS precursors specifically, activation in CO or CO–H_2 are common practice.

It should be noted here that many authors explicitly conclude that sintering is not playing a significant part in the deactivation of Fe catalysts.[93,174,206]

Deactivation through poisoning

Sulfur poisoning in iron-based FTS catalysts is widely reported in the literature. Bartholomew and Bowman[181] studied the effect of H_2S on the catalytic performance of cobalt and iron FTS catalysts. Upon addition of H_2S, they observed a decline in catalyst activity while the selectivity remained unaffected. This behaviour is commonly observed. Sulfur is thought to deactivate the FTS catalysts through the physical inhibition of active surface sites. At higher sulfur contents, also multilayer sulfur compounds are reported.[181] Chaffee *et al.*[182] observed significant deactivation when H_2S was added to the syngas feed. Their Fe–Mn co-precipitated catalyst was reported to be more resistant to sulfur poisoning. The authors claimed that this was due to the fast formation of MnOS compounds, thereby protecting the iron phase from deactivation. Dry[1] and later Duvenhage *et al.*[80,87] reported sulfur poisoning in large scale fixed bed reactors. More specifically, it was found that mainly the entrance of the catalyst bed was poisoned by sulfur with the rest of the bed remaining unaffected. Liu *et al.*[107] specifically investigated the effect of carbonyl sulfide (COS) on the catalyst performance. They concluded that the catalyst activity was decreased significantly, while the selectivity towards lighter FTS products (CH_4–C_4) was increased.

Interestingly, many groups found positive effects from sulfur at lower concentrations. Bartholomew and Bowman[181] reported that iron boride catalysts were very resistant to sulfur poisoning even at high sulfur contents, while low sulfur contents were observed to increase the catalyst activity. Similar conclusions were drawn by Madon and Shaw for iron carbides.[61] They found that the carburized iron FTS catalysts required twice the amount of sulfur compared to reduced iron catalysts. Addition of small amounts of H_2S to the syngas feed was observed to improve activity and the C_{5+} selectivity of the catalysts. This was confirmed much later in papers by Bromfield and Coville,[196] and Wu *et al.*[62] The groups found that small amounts of sulfur, most likely present in the form of sulfates, improved the reducibility of the iron catalyst by either dispersing the iron phase or helping with the removal of iron lattice oxygen atoms.

Sulfur promotion has been known in the literature for quite some time. Except for increased catalyst activity,[62,196,207,208] reported promotion effects include improved selectivity[140,183,198–201,207,209] and stability.[183,198] The enhanced olefin selectivity upon addition of small quantities of sulfur has in fact been reported in patent literature as early as 1929.[199–201] Van Dijk *et al.*[198] and Kritzinger[183] later reported the increased olefin selectivity upon addition of small amounts of sulfur. Van Dijk *et al.*[198] concluded that treatment of an iron catalyst with small amounts of ammonium sulfate increased catalyst stability and the selectivity towards short olefin chains at the expense of methane. Kritzinger[183] studied the effect of small amounts of sulfur to a commercial FTS plant. He hypothesized that the positive effect on the olefinicity of the products might be due to the selective poisoning of highly active sites, which would inhibit the hydrogenation of surface olefin species. Furthermore, it was concluded that even upon addition of sulfur levels 10–15 times higher than normally allowed under plant operation, no significant negative effects were observed on the catalyst performance. In addition, catalyst stability was improved upon addition of H_2S, an effect that was attributed to the possible stabilization of the χ-Fe_5C_2 carbide phase in a similar way that H_2S prevents metal dusting in reformers.[210]

Conclusions and outlook

Even after more than 80 years of research on iron-based Fischer–Tropsch synthesis catalysts, the system continues to be a challenge for scientists who work on unraveling its working mechanisms. The complex chemical structure of the iron catalysts and the dynamic nature of the iron–carbon–oxygen system under FTS conditions complicate any straightforward interpretation of structure–catalytic performance relationships. This is illustrated by the many mechanisms and active sites that have been proposed in the past and reviewed in this article. It has been shown that catalyst deactivation is an incredibly multifaceted process. In the real catalytic process, most probably, all of the discussed deactivation mechanisms mentioned to some extent play a role in the overall decreasing activity of the catalysts with time-on-stream.

Surely, at high syngas conversion, oxidation of the active phases by the high partial pressure of water and carbon dioxide produced in the FTS reaction plays an important role in deactivation of the catalysts. Also, a collapse of the high surface area of the catalysts as a result of sintering of the active phase, facilitated by high partial pressures of water, may play an important part in the overall deactivation process. Many studies have shown that carbon build-up on the surface of the catalyst, in the form of hydrocarbons which can form a reactant diffusion barrier or inactive carbon physically blocking active sites, can be an important factor in deactivation as well. Sometimes, more specifically, pore blocking by carbonaceous deposits is reported as well, resulting in a drastic drop in accessible catalytic surface area. Sulfur or other catalyst

poisons can further decrease catalytic activity and especially industrially this is an important factor to take into account in commercial catalyst design.

From the first characterization studies onward, scientists have tried to correlate bulk phase compositions with the catalytic behaviour of the catalyst materials. Undoubtedly, bulk phases do play an important role in determining the surface structure of the catalyst, and thereby its catalytic behaviour. It should be stressed, however, that the typical timescales of surface reconstruction and bulk phase reorganization can be very different. Furthermore, if one would assign a certain surface composition of carbon, hydrogen and iron to be the active site, one can easily recognize that competition between the surface polymerization reaction taking place on that active site and the diffusion of reactants into the bulk to induce a phase change can significantly delay the observation of such phase changes. Therefore, the observation of changes in catalytic performance is seldom paralleled by the observation of changes in bulk composition of the catalysts. This bulk–surface disagreement is often reflected in the ambiguous conclusions that are drawn from studies applying mainly surface sensitive techniques (*e.g.* XPS, AES) and studies that apply techniques that are typically sensitive for the bulk composition of the catalyst (*e.g.* MES, XRD).

Another important factor which complicates the direct interpretation of deactivation phenomena taking place in the catalyst is the wide range of pretreatments that are used to activate the catalyst material. Many specific pretreatment studies have shown that certain activation treatments may lead to improved catalyst activity, selectivity and stability. Because the exact underlying structural and electronic causes for the improved catalyst performance as a result of a certain treatment are not always clear, it is not always possible to identify specific deactivation pathways. Very often the conclusions that are drawn from different studies of identical catalysts are very different and sometimes they are even found to contradict each other. Related to this, it is often found that the synthesis of an active, selective and most importantly, stable iron-based FTS catalyst is not always easy to reproduce. Different studies of catalysts of identical chemical composition pretreated under similar conditions often yield different catalytic performance. Detailed catalyst preparation and characterization studies or efforts to synthesize well-characterized model catalysts are scarce, possibly owing to the industrial background and trial-and-error based approach for the synthesis of early FTS catalysts. It is therefore recommended that more studies are concentrated on the development of reproducible, well-characterized representative (model) catalysts. A final, maybe somewhat straightforward point to be made here is that, in industrial Fischer–Tropsch synthesis, different reactors, each with their own specific process parameters, will have their own specific deactivation pathways. A slurry phase or fluidized bed reactor obviously suffer higher deactivation rates as a result of breakup of catalyst particles by attrition and/or carburization than a fixed bed reactor. On the other hand, fixed bed reactors may be more prone to catalyst oxidation near the reactor exit as a result of higher partial pressures of water and carbon dioxide products.

The recent renewed interest in iron-based FTS catalysts has boosted efforts to elucidate its working and deactivation mechanisms. New catalyst characterization tools are constantly developed and older techniques have been improved. Perhaps the most interesting and promising developments in catalyst characterization are the increasing applications of techniques *in situ*. The *in situ* approach enables researchers to study the catalyst during the different stages of catalyst pretreatments and during FTS, sometimes even at near industrial conditions, thereby gaining important insights into the structure–activity relationships in the "working" catalyst. To summarize, in order to gain more insight into the structure–performance relationship in iron-based FTS catalysts, three areas of research can be recommended for further focus:

1. Development of a reproducible, better defined, model iron catalyst system;
2. Combined surface and bulk characterization studies; and
3. Development and application of *in situ* characterization tools.

Research efforts that are able to combine these three areas are the most promising efforts to benefit the understanding of the activation and deactivation mechanisms in iron-based FTS catalysts in the years to come.

References

1 M. E. Dry, *Catal. Lett*., 1990, **7**, 241–251.
2 H. Schulz, *Appl. Catal., A*, 1999, **186**, 3–12.
3 I. I. Rahmim, *Oil Gas J*., 2008, **106**, 23–28.
4 Literature survey based on journal articles and patents in the CAS database mentioning the concept "Fischer–-Tropsch".
5 M. Boudart, *Top. Catal*., 1994, **1**, 405–414.
6 R. M. Cornell and U. Schwertmann, *The Iron Oxides: Structure, Properties, Reactions, Occurrences and Uses*, Wiley-VCH, Weinheim, 1996.
7 R. M. Cornell and U. Schwertmann, in *The Iron Oxides: Structure, Properties, Reactions, Occurrences and Uses*, Wiley-VCH, Weinheim, 1996, p. 488.
8 C. D. Frohning, in *Fischer-Tropsch Synthese, Chemierohstoffe aus Kohle*, ed. J. Falbe, Thieme, Stuttgart, 1977.
9 H. H. Storch, N. Golumbic and R. B. Anderson, *The Fischer-Tropsch and Related Syntheses*, John Wiley & Sons, Inc., New York, 1951.
10 M. E. Dry, in *Catalysis - Science and Technology*, ed. J. R. Anderson and M. Boudart, Springer-Verlag, New York, 1981, vol. 1, pp. 160–255.
11 J. L. Rendon and C. J. Serna, *Clay Miner*., 1981, **16**, 375–381.
12 J. E. Iglesias, A. M. Ocantilde and C. J. Serna, *Appl. Spectrosc*., 1990, **44**, 418–426.
13 D. S. Newsome, *Catal. Rev. Sci. Eng*., 1980, **21**, 275–318.
14 H.-B. Zhang and G. L. Schrader, *J. Catal*., 1985, **95**, 325–332.
15 D. G. Rethwisch and J. A. Dumesic, *J. Catal*., 1986, **101**, 35–42.
16 E. S. Lox and G. F. Froment, *Ind. Eng. Chem. Res*., 1993, **32**, 61–70.
17 K. Rao, F. E. Huggins, V. Mahajan, G. P. Huffman and V. U. S. Rao, *Hyperfine Interact*., 1994, **93**, 1745–1749.
18 K. R. P. M. Rao, F. E. Huggins, V. Mahajan, G. P. Huffman, V. U. S. Rao, B. L. Bhatt, D. B. Bukur, B. H. Davis and R. J. O'Brien, *Top. Catal*., 1995, **2**, 71–78.
19 F. Blanchard, J. P. Reymond, B. Pommier and S. J. Teichner, *J. Mol. Catal*., 1982, **17**, 171–181.
20 J. P. Reymond, P. Meriaudeau and S. J. Teichner, *J. Catal*., 1982, **75**, 39–48.
21 C. S. Kuivila, P. C. Stair and J. B. Butt, *J. Catal*., 1989, **118**, 299–311.
22 J. B. Butt, *Catal. Lett*., 1991, **7**, 61–81.
23 P. Tarte, J. Prudhomme, F. Jeannot and O. Evrard, *C. R. Hebd. Seances Acad. Sci. Paris*, 1969, **269C**, 1529–1531.

24 G. W. Poling, *J. Electrochem. Soc.*, 1969, **116**, 958–963.
25 R. M. Taylor and U. Schwertmann, *Clay Miner.*, 1974, **10**, 299–310.
26 C. H. Rochester and S. A. Topham, *J. Chem. Soc., Faraday Trans. 1*, 1979, **75**, 1073–1088.
27 P. Cambier, *Clay Miner.*, 1986, **21**, 191–200.
28 A. Raman, B. Kuban and A. Razvan, *Corros. Sci.*, 1991, **32**, 1295–1306.
29 G. Busca, V. Lorenzelli, G. Ramis and R. J. Willey, *Langmuir*, 1993, **9**, 1492–1499.
30 D. Thierry, D. Persson, C. Leygraf, D. Delichere, S. Joiret, C. Pallotta and A. Hugotlegoff, *J. Electrochem. Soc.*, 1988, **135**, 305–310.
31 D. L. A. de Faria, S. V. Silva and M. T. de Oliveira, *J. Raman Spectrosc.*, 1997, **28**, 873–878.
32 N. S. McIntyre and D. G. Zetaruk, *Anal. Chem.*, 1977, **49**, 1521–1529.
33 K. Wandelt, *Surf. Sci. Rep.*, 1982, **2**, 1–121.
34 S. Z. Li, R. J. O'Brien, G. D. Meitzner, H. Hamdeh, B. H. Davis and E. Iglesia, *Appl. Catal., A*, 2001, **219**, 215–222.
35 M. Wilke, F. Farges, P. E. Petit, G. E. Brown and F. Martin, *Am. Mineral.*, 2001, **86**, 714–730.
36 J. Prietzel, J. Thieme, K. Eusterhues and D. Eichert, *Eur. J. Soil Sci.*, 2007, **58**, 1027–1041.
37 E. Murad and J. H. Johnston, in *Mössbauer Spectroscopy Applied to Inorganic Chemistry*, ed. G. Long, Plenum Publ. Corp., New York, 1987, vol. 2, pp. 507–582.
38 G. M. da Costa, E. de Grave, L. H. Bowen, R. E. Vandenberghe and P. M. A. de Bakker, *Clays Clay Miner.*, 1994, **42**, 628–633.
39 A. J. H. M. Kock and J. W. Geus, *Prog. Surf. Sci.*, 1985, **20**, 165–272.
40 H. P. Bonzel and H. J. Krebs, *Surf. Sci.*, 1980, **91**, 499–513.
41 J. A. Bearden and A. F. Burr, *Rev. Mod. Phys.*, 1967, **39**, 125–142.
42 G. B. Raupp and W. N. Delgass, *J. Catal.*, 1979, **58**, 348–360.
43 M. Pijolat, V. Perrichon and P. Bussière, *J. Catal.*, 1987, **107**, 82–91.
44 E. K. Storms, *The Refractory Carbides*, Academic Press, New York, 1967.
45 L. E. Toth, *Transition Metal Carbides and Nitrides*, Academic Press, New York, 1971.
46 S. T. Oyama, *Catal. Today*, 1992, **15**, 179–200.
47 N. Engel, *Powder Metall. Bull.*, 1954, **7**, 8–18.
48 L. Brewer, *Science*, 1968, **161**, 115–122.
49 L. Ramqvist, K. Hamrin, G. Johansson, A. Fahlman and C. Nordling, *J. Phys. Chem. Solids*, 1969, **30**, 1835–1847.
50 L. Ramqvist, K. Hamrin, G. Johansson, U. Gelius and C. Nordling, *J. Phys. Chem. Solids*, 1970, **31**, 2669–2672.
51 L. Ramqvist, B. Ekstig, E. Kallne, E. Noreland and R. Manne, *J. Phys. Chem. Solids*, 1969, **30**, 1849–1860.
52 R. B. Levy and M. Boudart, *Science*, 1973, **181**, 547–549.
53 S. T. Oyama and G. L. Haller, in *Catalysis, Specialist Periodical Reports*, ed. G. C. Bond and G. Webb, The Chemical Society, London, 1981, vol. 5, p. 333.
54 S. T. Oyama, *The Chemistry of Transition Metal Carbides and Nitrides*, Blackie Academic and Professional, Glasgow, 1996.
55 J. G. Chen, *Chem. Rev.*, 1996, **96**, 1477–1498.
56 L. Leclercq, in *Surface Properties and Catalysis by Nonmetals*, ed. J. P. Bonnelle, B. Delmon and E. Derouane, Reidel, Dordrecht, 1983, p. 433.
57 L. Leclercq, K. Imura, S. Yoshida, T. Barbee and M. Boudart, in *Preparation of Catalysts II*, ed. B. Delmon, P. Grange, P. A. Jacobs and G. Poncelet, Elsevier, Amsterdam, 1978, p. 627.
58 J. F. Shultz, F. S. Karn and R. B. Anderson, *Report of Investigation 6974*, US Bureau of Mines, 1967.
59 M. Saito and R. B. Anderson, *J. Catal.*, 1980, **63**, 438–446.
60 J. W. Dun, E. Gulari and K. Y. S. Ng, *Appl. Catal.*, 1985, **15**, 247–263.
61 R. J. Madon and H. Shaw, *Catal. Rev. Sci. Eng.*, 1977, **15**, 69.
62 B. Wu, L. Bai, H. Xiang, Y.-W. Li, Z. Zhang and B. Zhong, *Fuel*, 2004, **83**, 205–212.
63 J. F. Shultz, L. J. E. Hofer, K. C. Stein and R. B. Anderson, *Bull. – U. S., Bur. Mines*, 1963, **612**, 1–70.
64 O. G. Malan, J. D. Louw and L. C. Ferreira, *Brennst.–Chem.*, 1961, **42**, 209–212.
65 J. P. Senateur, R. Fruchart and A. Michel, *C. R. Acad. Sci. (Paris)*, 1963, **255**, 1615.
66 J. P. Senateur and R. Fruchart, *C. R. Acad. Sci. (Paris)*, 1963, **256**, 3114.
67 H. C. Eckstrom and W. A. Adcock, *J. Am. Chem. Soc.*, 1950, **72**, 1042–1043.
68 F. H. Herbstein and J. A. Snyman, *Inorg. Chem.*, 1964, **3**, 894–896.
69 G. H. Barton and B. Gale, *Acta Crystallogr.*, 1964, **17**, 1460–1462.
70 J. W. Niemantsverdriet, A. M. van der Kraan, W. L. van Dijk and H. S. van der Baan, *J. Phys. Chem.*, 1980, **84**, 3363–3370.
71 M. Dirand and L. Afqir, *Acta Metall.*, 1983, **31**, 1089–1107.
72 G. Le Caër, J. M. Dubois, M. Pijolat, V. Perrichon and P. Bussière, *J. Phys. Chem.*, 1982, **86**, 4799–4808.
73 E. M. Cohn and L. J. E. Hofer, *US Pat.*, 2,535,042, 1950.
74 L. J. E. Hofer and E. M. Cohn, *J. Chem. Phys.*, 1950, **18**, 766.
75 R. B. Anderson, L. J. E. Hofer, E. M. Cohn, H. Steiner, M. Greyson and S. W. Weller, in *Catalysis*, ed. P. H. Emmett, Reinhold, New York, 1956, vol. 4.
76 J. F. Shultz, L. J. E. Hofer, E. M. Cohn, K. C. Stein and R. B. Anderson, *Bull. – U. S., Bur. Mines*, 1959, **578**, 50.
77 J. Galuszka, T. Sano and J. A. Sawicki, *J. Catal.*, 1992, **136**, 96–109.
78 A. Machocki, *Appl. Catal.*, 1991, **70**, 237–252.
79 H. Jung and W. J. Thomson, *J. Catal.*, 1992, **134**, 654–667.
80 D. J. Duvenhage, R. L. Espinoza and N. J. Coville, in *Catalyst Deactivation 1994*, ed. B. Delmon and G. F. Froment, Elsevier, Amsterdam, 1994, vol. 88, pp. 351–358.
81 D. B. Bukur, M. Koranne, X. S. Lang, K. Roa and G. P. Huffman, *Appl. Catal., A*, 1995, **126**, 85–113.
82 D. B. Bukur, L. Nowicki and X. S. Lang, *Energy Fuels*, 1995, **9**, 620–629.
83 D. B. Bukur, L. Nowicki, R. K. Manne and X. S. Lang, *J. Catal.*, 1995, **155**, 366–375.
84 D. B. Bukur, K. Okabe, M. P. Rosynek, C. P. Li, D. J. Wang, K. Rao and G. P. Huffman, *J. Catal.*, 1995, **155**, 353–365.
85 N. B. Jackson, A. K. Datye, L. Mansker, R. J. O'Brien and B. H. Davis, in *Catalyst Deactivation 1997*, ed. C. H. Bartholomew and G. A. Fuentes, Elsevier, Amsterdam, 1997, vol. 111, pp. 501–516.
86 Y. Jin and A. K. Datye, in *Natural Gas Conversion V*, ed. A. Parmaliana, D. Sanfilippo, F. Frusteri, A. Vaccari and F. Arena, Elsevier, Amsterdam, 1998, vol. 119, pp. 209–214.
87 D. J. Duvenhage and N. J. Coville, *Appl. Catal., A*, 2006, **298**, 211–216.
88 W. S. Ning, N. Koizumi, H. Chang, T. Mochizuki, T. Itoh and M. Yamada, *Appl. Catal., A*, 2006, **312**, 35–44.
89 H. Hayakawa, H. Tanaka and K. Fujimoto, *Appl. Catal., A*, 2006, **310**, 24–30.
90 L. D. Mansker, Y. M. Jin, D. B. Bukur and A. K. Datye, *Appl. Catal., A*, 1999, **186**, 277–296.
91 R. A. Dictor and A. T. Bell, *J. Catal.*, 1986, **97**, 121–136.
92 G. B. Raupp and W. N. Delgass, *J. Catal.*, 1979, **58**, 337–347.
93 G. B. Raupp and W. N. Delgass, *J. Catal.*, 1979, **58**, 361–369.
94 H. Matsumoto and C. O. Bennett, *J. Catal.*, 1978, **53**, 331–344.
95 H. Itoh, H. Hosaka, T. Ono and E. Kikuchi, *Appl. Catal.*, 1988, **40**, 53–66.
96 Q.-L. Hao, F.-X. Liu, H. Wang, J. Chang, C.-H. Zhang, L. Bai, H.-W. Xiang, Y.-W. Li, F. Yi and B.-F. Xu, *J. Mol. Catal. A: Chem.*, 2007, **261**, 104–111.
97 R. A. Diffenbach and D. J. Fauth, *J. Catal.*, 1986, **100**, 466–476.
98 D. S. Kalakkad, M. D. Shroff, S. Kohler, N. Jackson and A. K. Datye, *Appl. Catal., A*, 1995, **133**, 335–350.
99 N. Sirimanothan, H. H. Hamdeh, Y. Q. Zhang and B. H. Davis, *Catal. Lett.*, 2002, **82**, 181–191.
100 Y. M. Jin, H. F. Xu and A. K. Datye, *Microsc. Microanal.*, 2006, **12**, 124–134.
101 J. A. Amelse, J. B. Butt and J. H. Schwartz, *J. Phys. Chem.*, 1978, **82**, 558–563.
102 L. Guczi and K. Lázár, *Catal. Lett.*, 1990, **7**, 53–60.
103 K. Lazar, Z. Schay and L. Guczi, *J. Mol. Catal.*, 1982, **17**, 205–218.
104 Y. Q. Zhang, N. Sirimanothan, R. J. O'Brien, H. H. Hamdeh and B. H. Davis, *Stud. Surf. Sci. Catal.*, 2001, **139**, 125–132.

105 R. J. Gormley, M. F. Zarochak, P. W. Deffenbaugh and K. Rao, *Appl. Catal., A*, 1997, **161**, 263–279.
106 A. Loaiza-Gil, B. Fontal, F. Rueda, J. Mendialdua and R. Casanova, *Appl. Catal., A*, 1999, **177**, 193–203.
107 Z.-T. Liu, Z. Jing-Lai and Z. Bi-Jiang, *J. Mol. Catal.*, 1994, **94**, 255–261.
108 M. V. Cagnoli, S. G. Marchetti, N. G. Gallegos, A. M. Alvarez, A. A. Yeramian and R. C. Mercader, *Mater. Chem. Phys.*, 1991, **27**, 403–418.
109 L. M. Tau, S. Borcar, D. Bianchi and C. O. Bennett, *J. Catal.*, 1984, **87**, 36–54.
110 D. Bianchi, S. Borcar, F. Teule-Gay and C. O. Bennett, *J. Catal.*, 1983, **82**, 442–456.
111 D. Mahajan, P. Gutlich, J. Ensling, K. Pandya, U. Stumm and P. Vijayaraghavan, *Energy Fuels*, 2003, **17**, 1210–1221.
112 D. J. Dwyer and J. H. Hardenbergh, *J. Catal.*, 1984, **87**, 66–76.
113 H. J. Krebs, H. P. Bonzel and G. Gafner, *Surf. Sci.*, 1979, **88**, 269–283.
114 D. J. Dwyer and G. A. Somorjai, *J. Catal.*, 1978, **52**, 291–301.
115 U. M. Graham, A. Dozier, R. A. Khatri, R. Srinivasan and B. H. Davis, *Stud. Surf. Sci. Catal.*, 2007, **163**, 101–124.
116 N. S. Kopelev, V. Chechersky, A. Nath, Z. L. Wang, E. Kuzmann, B. Zhang and G. H. Via, *Chem. Mater.*, 1995, **7**, 1419–1421.
117 S. Takenaka, M. Serizawa and K. Otsuka, *J. Catal.*, 2004, **222**, 520–531.
118 H. Yamashita, Y. Ohtsuka, S. Yoshida and A. Tomita, *Energy Fuels*, 1989, **3**, 686–692.
119 M. D. Shroff and A. K. Datye, *Catal. Lett.*, 1996, **37**, 101–106.
120 J. Xu and C. H. Bartholomew, *J. Phys. Chem. B*, 2005, **109**, 2392–2403.
121 H. Kölbel and M. Ralek, *Catal. Rev. Sci. Eng.*, 1980, **21**, 225–274.
122 H. Bluhm, M. Havecker, A. Knop-Gericke, M. Kiskinova, R. Schlogl and M. Salmeron, *MRS Bull.*, 2007, **32**, 1022–1030.
123 J. J. Retief, *Powder Diffr.*, 1999, **14**, 130–132.
124 G. Le Caër, J. M. Dubois and J. P. Senateur, *J. Solid State Chem.*, 1976, **19**, 19–28.
125 J. W. Niemantsverdriet and A. M. van der Kraan, *J. Catal.*, 1981, **72**, 385–388.
126 R. T. K. Baker, *Catal. Rev. Sci. Eng.*, 1979, **19**, 161–209.
127 M. A. Vannice, *J. Catal.*, 1975, **37**, 462–473.
128 J. Kleefeld and L. L. Levenson, *Thin Solid Films*, 1979, **64**, 389–393.
129 S. R. Shatynski, *Oxid. Met.*, 1979, **13**, 105–118.
130 T. Grzybek, H. Papp and M. Baerns, *Appl. Catal.*, 1987, **29**, 351–359.
131 D. P. Shashkin, P. A. Shiryaev, A. V. Chichagov, O. S. Morozova and O. V. Krylov, *Kinet. Catal.*, 1992, **33**, 744–749.
132 M. D. Shroff, D. S. Kalakkad, K. E. Coulter, S. D. Kohler, M. S. Harrington, N. B. Jackson, A. G. Sault and A. K. Datye, *J. Catal.*, 1995, **156**, 185–207.
133 H. Matsumoto, *J. Catal.*, 1984, **86**, 201–204.
134 F. Fischer and H. Tropsch, *Brennst.–Chem.*, 1923, **4**, 276–285.
135 F. Fischer and H. Tropsch, *Brennst.–Chem.*, 1926, **7**, 97–116.
136 M. E. Dry, *International Conference on Catalysis and Catalytic Processing*, Cape Town, South Africa, 1993, pp. 57–66.
137 A. T. Bell, *Catal. Rev. Sci. Eng.*, 1981, **23**, 203–232.
138 V. Ponec, *Catal. Rev. Sci. Eng.*, 1978, **18**, 151–171.
139 R. B. Anderson, *Catalysts for the Fischer–Tropsch Synthesis*, Van Nostrand Reinhold, New York, 1956.
140 R. B. Anderson, *The Fischer–Tropsch Synthesis*, Academic Press, New York, 1984.
141 J. P. Hindermann, G. J. Hutchings and A. Kiennemann, *Catal. Rev. Sci. Eng.*, 1993, **35**, 1–127.
142 M. E. Dry, *Appl. Catal., A*, 1996, **138**, 319–344.
143 A. A. Adesina, *Appl. Catal., A*, 1996, **138**, 345–367.
144 G. P. Van der Laan and A. A. C. M. Beenackers, *Catal. Rev. Sci. Eng.*, 1999, **41**, 255–318.
145 R. C. Brady and R. Pettit, *J. Am. Chem. Soc.*, 1981, **103**, 1287–1289.
146 B. H. Davis, *Fuel Process. Technol.*, 2001, **71**, 157–166.
147 P. Biloen, J. N. Helle and W. M. H. Sachtler, *J. Catal.*, 1979, **58**, 95–107.
148 B. W. Wojciechowski, *Catal. Rev. Sci. Eng.*, 1988, **30**, 629–702.
149 H. Schulz, E. v. Steen and M. Claeys, *Selective Hydrogenation and Dehydrogenation*, DGMK, Kassel, 1993.
150 E. L. Muetterties and J. Stein, *Chem. Rev.*, 1979, **79**, 479–490.
151 M. A. Vannice, *Catal. Rev. Sci. Eng.*, 1976, **14**, 153–191.
152 G. A. Huff, Jr and C. N. Satterfield, *Ind. Eng. Chem. Proc. Des. Dev.*, 1984, **23**, 696–705.
153 J. F. Kummer and P. H. Emmett, *J. Am. Chem. Soc.*, 1953, **75**, 5177–5183.
154 W. K. Hall, R. J. Kokes and P. H. Emmett, *J. Am. Chem. Soc.*, 1960, **82**, 1027–1037.
155 W. K. Hall, R. J. Kokes and P. H. Emmett, *J. Am. Chem. Soc.*, 1957, **79**, 2983–2989.
156 J. T. Kummer and P. H. Emmett, *J. Am. Chem. Soc.*, 1953, **75**, 5177–5183.
157 J. T. Kummer, H. H. Podgurski, W. B. Spencer and P. H. Emmett, *J. Am. Chem. Soc.*, 1951, **73**, 564–569.
158 G. Blyholder and P. H. Emmett, *J. Phys. Chem.*, 1959, **63**, 962–965.
159 I. Wender, S. Friedman, W. A. Steiner and R. B. Anderson, *Chem. Ind. (London, U. K.)*, 1958, 1694.
160 H. Pichler and H. Schulz, *Chem. Ing. Tech.*, 1970, **42**, 1162–1174.
161 G. Henrici-Olivé and S. Olivé, *Angew. Chem., Int. Ed. Engl.*, 1976, **15**, 136–141.
162 C. Masters, *Adv. Organomet. Chem.*, 1979, **17**, 61–103.
163 F. Domka and M. Z. Laniecki, *Z. Anorg. Allg. Chem.*, 1977, **435**, 273–283.
164 M. Kung and H. Kung, *Surf. Sci.*, 1981, **104**, 253–269.
165 C. R. F. Lund and J. A. Dumesic, *J. Phys. Chem.*, 1981, **85**, 3175–3180.
166 S. Oki and R. Mezaki, *J. Phys. Chem.*, 1973, **77**, 447–452.
167 D. G. Rethwisch and J. A. Dumesic, *J. Catal.*, 1986, **101**, 35–42.
168 T. van Herwijnen and W. A. de Jong, *J. Catal.*, 1980, **63**, 83–93.
169 J. E. Kubsh, Y. Chen and J. A. Dumesic, *J. Catal.*, 1981, **71**, 192–200.
170 M. Tinker and J. A. Dumesic, *J. Catal.*, 1987, **103**, 65.
171 C. H. Bartholomew, M. W. Stoker, L. Mansker and A. Datye, *Stud. Surf. Sci. Catal.*, 1999, **126**, 265–272.
172 A. P. Raje, R. J. O'Brien, L. G. Xu and B. H. Davis, *Stud. Surf. Sci. Catal.*, 1997, **111**, 527–533.
173 S. A. Eliason and C. H. Bartholomew, *Stud. Surf. Sci. Catal.*, 1997, **111**, 517–526.
174 S. A. Eliason and C. H. Bartholomew, *Appl. Catal., A*, 1999, **186**, 229–243.
175 H. P. Bonzel and H. J. Krebs, *Surf. Sci.*, 1982, **117**, 639–658.
176 A. P. B. Sommen, F. Stoop and K. Van Der Wiele, *Appl. Catal.*, 1985, **14**, 277–288.
177 J. S. Hwang, K. W. Jun and K. W. Lee, *Appl. Catal., A*, 2001, **208**, 217–222.
178 M. A. McDonald, D. A. Storm and M. Boudart, *J. Catal.*, 1986, **102**, 386–400.
179 M. E. Dry, T. Shingles and C. S. van H. Botha, *J. Catal.*, 1970, **17**, 341–346.
180 M. E. Dry, T. Shingles, L. J. Boshoff and C. S. van H. Botha, *J. Catal.*, 1970, **17**, 347–354.
181 C. H. Bartholomew and R. M. Bowman, *Appl. Catal.*, 1985, **15**, 59–67.
182 A. L. Chaffee, I. Campbell and N. Valentine, *Appl. Catal.*, 1989, **47**, 253–276.
183 J. A. Kritzinger, *Catal. Today*, 2002, **71**, 307–318.
184 R. B. Anderson, F. S. Karn and J. F. Shultz, *Bull. – U. S., Bur. Mines*, 1964, **614**, 29–39.
185 L. C. Rubin and H. G. McGrath, *US Pat.*, 2,620,346, 1952.
186 A. Voorhies Jr, *US Pat.*, 2,533,072, 1950.
187 L. I. Griffin Jr, *US Pat.*, 2,487,867, 1949.
188 H. A. Wright, *US Pat.*, 6,486,220, 2002.
189 E. Ruckensten, *Metal–Support Interactions in Catalysis, Sintering, and Redispersion*, ed. S. A. Stevenson, J. A. Dumesic, R. T. A. Baker and E. Ruckenstein, Van Nostrand Reinhold Company, Boston, 1987, p. 141.
190 H. Kölbel and H. Giehring, *Brennst.–Chem.*, 1963, **44**, 343.
191 B. Jager and R. Espinoza, *Catal. Today*, 1995, **23**, 17–28.
192 M. E. Dry, in *Catalysis - Science and Technology*, ed. J. R. Anderson and M. Boudart, Springer-Verlag, New York, 1981, vol. 1, p. 198.

193 V. U. S. Rao, G. J. Stiegel, G. J. Cinquegrane and R. D. Srivastava, *Fuel Process. Technol.*, 1992, **30**, 83–107.
194 M. E. Dry, in *Applied Industrial Catalysis*, ed. B. E. Leach, Academic Press, New York, 1983, vol. 2, p. 167.
195 C. D. Frohning, in *New Synthesis with Carbon Monoxide*, ed. J. Falbe, Springer-Verlag, New York, 1980.
196 T. C. Bromfield and N. J. Coville, *Appl. Catal., A*, 1999, **186**, 297–307.
197 R. A. Dalla Betta, A. G. Piken and M. Shelef, *J. Catal.*, 1975, **40**, 173–183.
198 W. L. van Dijk, J. W. Niemantsverdriet, A. M. van dar Kraan and H. S. van der Baan, *Appl. Catal.*, 1982, **2**, 273–288.
199 IG Farbenindustrie AG, *Br. Pat.*, 322,284, 1929.
200 E. T. Layng, *US Pat.*, 2,446,426, 1948.
201 W. W. Myddleton, *Br. Pat.*, 509,325, 1939.
202 F. Fischer, *Brennst.–Chem.*, 1935, **16**, 1–11.
203 H. J. Jung, P. L. Walker and A. Vannice, *J. Catal.*, 1982, **75**, 416–422.
204 M. E. Dry, T. Shingles and L. J. Boshoff, *J. Catal.*, 1972, **25**, 99–104.
205 D. B. Bukur, X. Lang, J. A. Rossin, W. H. Zimmerman, M. P. Rosynek, E. B. Yeh and C. Lil, *Ind. Eng. Chem. Res.*, 1989, **28**, 1130–1140.
206 M. Perez-Cabero, E. Romeo, C. Royo, A. Monzon, A. Guerrero-Ruiz and I. Rodriguez-Ramos, *J. Catal.*, 2004, **224**, 197–205.
207 E. F. G. Herrington and L. A. Woodward, *Trans. Faraday Soc.*, 1939, **35**, 958–966.
208 H. R. Stenger, Jr. and C. N. Satterfield, *Ind. Eng. Chem. Proc. Des. Dev.*, 1985, **24**, 415–420.
209 R. J. Madon and W. F. Taylor, *Am. Chem. Soc. Adv. Chem. Ser.*, 1979, **178**, 93–112.
210 H. J. Grabke, *Corrosion*, 1995, **51**, 711–720.